

PREPARED FOR SUBMISSION TO JHEP

# Solvable Models of Heat Transport in Quantum Mechanics

---

R Loganayagam<sup>a</sup>, Prithvi Narayan<sup>b</sup> and Swathi T S<sup>b</sup>

<sup>a</sup>*International Centre for Theoretical Sciences (ICTS-TIFR),  
Tata Institute of Fundamental Research, Shivakote, Hesaraghatta, Bengaluru 560089, India.*

<sup>b</sup>*Department of Physics, Indian Institute of Technology, Palakkad 678557, India.*

*E-mail:* [nayagam@icts.res.in](mailto:nayagam@icts.res.in), [prithvi.narayan@gmail.com](mailto:prithvi.narayan@gmail.com),  
[swathisubramanian3@gmail.com](mailto:swathisubramanian3@gmail.com)

**ABSTRACT:** We investigate solvable models of heat transport between a pair of quantum mechanical systems initialized at two different temperatures. At time  $t = 0$ , a weak interaction is switched on between the systems, and we study the resulting energy transport. Focusing on the heat current as the primary observable, we analyze both the transient dynamics and the long-time behavior of the system. We demonstrate that simple toy models - including Random Matrix Theory like models (*RMT models*) and Schwarzian like models (*conformal models*) - can capture many generic features of heat transport, such as transient current peaks and the emergence of non-equilibrium steady state (NESS). For these models, we derive a variety of exact results characterizing the short time transients, long time approach to NESS and thermal conductivity. Finally, we show how these features appear in a more realistic solvable model, the Double-Scaled SYK (DSSYK) model. We demonstrate that the DSSYK model interpolates between the seemingly distinct toy models discussed earlier, with the toy models in turn providing a useful lens through which to understand the rich features of DSSYK.

---

## Contents

<b>1</b>	<b>Introduction</b>	<b>2</b>
<b>2</b>	<b>Setup for the heat transport and some toy models</b>	<b>7</b>
2.1	Description of the isolated quantum system	7
2.2	Heat transport between quantum systems	9
<b>3</b>	<b>Heat transport in toy models</b>	<b>12</b>
3.1	Toy Model 1 : Random Matrix Theory (RMT)	12
3.1.1	Cold Random Matrix Theory	17
3.2	Toy Model 2 : Conformal model	18
3.3	Toy Model 3 : Gaussian model	23
<b>4</b>	<b>Heat transport in DSSYK model</b>	<b>26</b>
4.1	Review of the double scaled SYK Model	26
4.1.1	Special Cases	32
4.2	Regimes in the DSSYK model	33
4.2.1	Conformal Regime	34
4.2.2	Cold RMT regime	35
4.3	Transport in DSSYK Models	37
4.3.1	DSSYK Model in the conformal regime $\lambda \rightarrow 0$	39
4.3.2	Numerical results for heat transport in DSSYK for $t < (1 - q)^{-\frac{3}{2}}$ and finite $\lambda$	40
<b>5</b>	<b>Conclusions and Outlook</b>	<b>43</b>
<b>A</b>	<b>Expression for energy current</b>	<b>44</b>
<b>B</b>	<b>Properties of <math>Z_k</math></b>	<b>45</b>
B.1	Long-Time Limit of the Two-Point Function $Z_k(\beta)$	46
<b>C</b>	<b>Additional details of DSSYK in conformal Regime</b>	<b>48</b>

---

# 1 Introduction

Transport is a well studied topic in physics, with relevance across a wide range of disciplines including statistical mechanics, condensed matter physics, fluid dynamics, and high energy physics. Measurements of transport properties—such as thermal and electrical conductivities—provide critical insights into the underlying structure and dynamics of physical systems. From a theoretical standpoint, transport constitutes one of the simplest and most accessible non-equilibrium processes, offering a natural bridge between theoretical predictions and experimental observations. As we will explore, key theoretical constructs such as two-point functions are directly related to experimentally measurable currents[1–4]. For all these reasons, transport studies have become an indispensable tool in physics.

In this work, we focus on one of the simplest scenario of heat transport : a pair of systems initialized at different temperatures are suddenly brought into contact, initiating an exchange of energy and setting up a heat current[5, 6]. The evolution typically proceeds through three stages: an initial transient regime at short times, an intermediate-time window characterized by a non-equilibrium steady state (NESS), and eventually at long times, thermalization to a common intermediate temperature.

Theoretical models that allow this entire transport process to be studied analytically are of fundamental importance. They serve not only as conceptual tools for testing physical intuition and identifying the mechanisms underlying observed phenomena, but also serve as essential testing grounds for broader ideas in non-equilibrium statistical mechanics. However, identifying exactly solvable models that capture all three stages of heat transport—transients, steady-state NESS, and thermalization poses a challenge. For instance, integrable systems are solvable, but do not thermalize in the standard sense [7, 8].

As for the NESS, in some exactly solvable theories, the exact NESS density matrix can be found [9, 10] and exact non-equilibrium heat currents can be computed in spin-chain models[11–14]. In weakly coupled theories, the heat transport can be captured by the Landauer formalism applied to quasiparticles (see [3, 15] for a review). However, even in these systems, it is hard to precisely describe the transients as well as the *approach* to NESS. Of course, in strongly coupled systems, there are no quasiparticles, and special methods like holography become necessary[16].

There is hence a need for solvable models that can access both transient and NESS regimes without relying on weak coupling or quasiparticles. In this work, we study a class of solvable models<sup>1</sup> that provide full control in these regimes.

---

<sup>1</sup>By solvable models, as will be clearer later in specific examples, we mean models where the two point function (and more generally, all correlation functions) are determined perhaps up to an integral.

In this work, we consider a pair of systems brought into thermal contact via operator couplings (for details see section 2) and study the heat current that flows from one to the other as a function of time. In the regime where the coupling between the two systems is weak, the heat current depends solely on the two-point function of the operator which couples the two systems, and we consider diverse systems in which the two point function is known explicitly.

We begin by analyzing transport between a pair of quantum systems which are described by simple toy models that allow full analytic control in the regimes of interest. We will consider three sets of toy models namely

- **Random matrix theory (RMT) model** (in section 3.1) : Here the system is described by a random matrix theory with following the well known Wigner semicircle.
- **Conformal model**(in section 3.2) : Here the system is taken to have two point function motivated from conformal symmetry (and also arising in some explicit models). While we do not have an explicit density of states here, we will later see that exponential density of states can give rise to these models.
- **Gaussian model**(in section 3.3) : Here the density of states is gaussian. This model can also arise as a special limit of the conformal model.

Despite their simplicity, one of the key results of our work is that these toy models already capture key qualitative features of the dynamics - a transient regime with a peak in the energy current followed by a relaxation into a non-equilibrium steady state obeying Fourier’s law where heat current is proportional to temperature difference. In each of the above models, we systematically characterize the transient regime (including the time at which heat current peaks and its height), the approach to the steady state (which may follow power law, exponential or gaussian behavior depending on the model) and the heat conductivity at NESS regime particularly its temperature dependence.

We then turn to a more realistic model the Sachdev-Ye-Kitaev (SYK) model in its double scaling limit, namely the Double Scaled SYK (DSSYK) model. The SYK model[17–19] has recently emerged as a paradigmatic example of a solvable, strongly interacting quantum systems. The model consists of  $N$  fermions with *disordered*  $p$  fermion interactions and becomes analytically tractable in the large- $N$  and at low energies[19, 20]. In this regime, the model exhibits many intriguing features that have attracted broad attention. The two-point functions become conformal, reflecting an emergent reparameterization symmetry[19, 20]. The system also displays strong

---

In all the examples we deal with in this work this turns out to be the case, since spectrum and matrix elements of operators are known.

quantum chaos, with a Lyapunov exponent saturating the universal bound[19, 21, 22], a hallmark of maximal chaos effectively captured by a low-energy Schwarzian theory. Furthermore, the model is believed to admit a holographic dual description, with the Schwarzian action corresponding to the boundary dynamics of nearly AdS<sub>2</sub> gravity[23, 24], making it a powerful toy model for exploring aspects of quantum gravity and holography. Motivated by the remarkable features outlined above, numerous studies have explored SYK variants, including extensions with higher symmetries [25–31] and supersymmetry [28, 32–34], among others. It is thus natural to ask what happens if the SYK model were used as the quantum system in our transport setup. This direction has been pursued in a number of works [6, 35, 36], where heat transport between coupled SYK systems was studied in various contexts. In [35], two SYK systems coupled via a channel were considered, and the resulting transport properties were analyzed. The authors found that the conductivity at intermediate temperatures follows a power-law dependence on temperature, with a distinct change in the exponent at a critical temperature. In [6], the authors derive general bounds on the rate of heat transfer in quantum systems, with implications for holography. For coupled SYK systems, they also numerically compute the energy flow and demonstrate eventual thermalization.

While the SYK model provides analytical control in the low-temperature and intermediate-time regime, at finite temperatures or during early-time transients the results are only numerical. To analytically study transport at finite temperatures, including the transient regime, it is necessary to consider a model that is solvable beyond these limits. To access these regimes, one considers the double scaling limit of the SYK model[37, 38], defined by  $N \rightarrow \infty$ ,  $p \rightarrow \infty$ , with  $\lambda \equiv \frac{2p^2}{N}$  held fixed. The resulting DSSYK model [38–40] is solvable at all temperatures and retains key features of the original SYK model in an appropriate limit. There has been a significant body of work on the DSSYK model, including the computation of correlation functions[39, 40], the analysis of multi-trace operator structures[41], and investigations into its implications for emergent gravitational dynamics[42–48]. In particular, its correlation functions can be given as an integral (or equivalently as an infinite sum) of certain special functions. As mentioned above, the conventional SYK physics is recovered in a particular limit termed *triple-scaling limit* where  $\lambda \rightarrow 0$  at low temperatures with  $T \sim \lambda^{\frac{3}{2}}$ [38]. The parameter  $\lambda$  plays a role somewhat analogous to the t’Hooft coupling : for small  $\lambda$ , the system is essentially free (although, at sufficiently low temperature, with  $T \sim \lambda^{\frac{3}{2}}$  the physics is nontrivial as we mentioned above) and at large  $\lambda$ , the theory is strongly coupled. As with the SYK model, numerous variants of the DSSYK model have also been investigated, including those with higher symmetries [49, 50] and supersymmetric versions [51].

With this background in place, we now turn to the next focus of this work: trans-

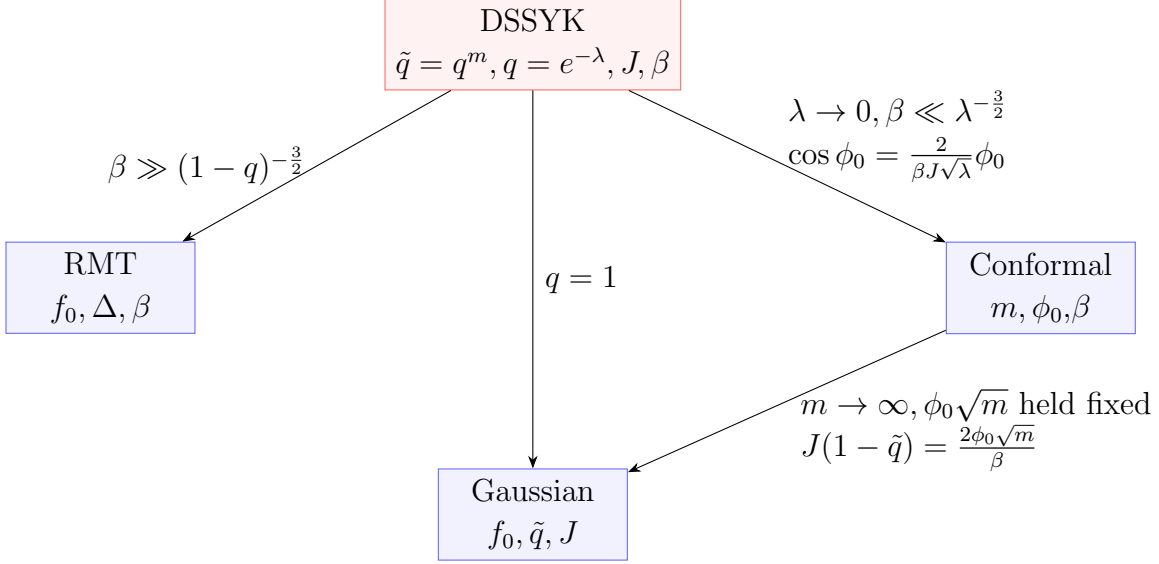


**Figure 1:** Relation between the DSSYK model and other toy models. Parameters of all the models and their relations are also given (see eq(4.26) for RMT and  $f_0 = 1$  for Gaussian model). See section 3 for the description of toy models and section 4.1 for the description of the DSSYK model.

port between two quantum systems, each described by a DSSYK model. The results obtained in earlier studies of coupled SYK systems is reproduced in appropriate regimes. For instance the power-law scaling of conductivity with respect to temperature observed in [35] is observed here as well; moreover our analytic results allow is to reliably calculate the prefactors that were previously computed only numerically. General bounds on energy transfer rates [6] are also explicitly verified. An added advantage of the DSSYK model is the presence of tunable parameters such as  $\lambda$  and the operator dimension  $m$ .

The DSSYK model stands out due to the availability of explicit results, we get additional insights : We find that the DSSYK system, even in isolation, is accurately described by simpler toy models introduced earlier in many regimes.

- We identify a characteriztic time scale,  $\tau_s$ , referred to as the *scrambling scale*, after which the dynamics matches that of the RMT model.
- We further see that DSSYK model reduces to the *RMT*, *Conformal*, and *Gaussian* models in appropriate limits of  $\beta$ ,  $\lambda$ , and  $q$ , as summarized in fig(1).
- The transition between conformal and RMT regime can also be realized by changing the temperature. In fact, loosely speaking, DSSYK exhibits a renormalization

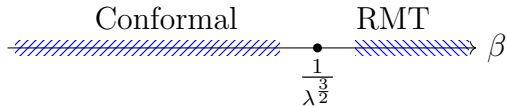


**Figure 2:** Schematic depiction of different regimes in the DSSYK model.

group (RG) flow between a UV theory described by a conformal model to an IR theory described by RMT model.

- The above point is most transparent in the  $\lambda \rightarrow 0$  regime, where we have the most analytic control and we observe the RMT to conformal crossover around  $\beta \sim \lambda^{-3/2}$  as shown in fig(2). At finite  $\lambda$ , this separation is less sharp, but a qualitative version of the flow persists : RMT region expands and we numerically<sup>2</sup> observe that there is still a conformal regime which shrinks as  $\lambda$  increases. The scenario we outline above is consistent with the  $\lambda \rightarrow \infty$  limit where the model reduces exactly to the RMT model.
- As we discuss later, the above statements translate directly into statements about transport. For the conductivity of the DSSYK model, we observe a smooth transition from the conformal to the RMT results as the temperature is varied, as shown in fig(23), consistent with the RG flow picture discussed above.

In section 2, we set up the computation of heat current and describe its properties. In subsections 3.1 and 3.2, we discuss the transport in the case of two toy models of interest namely the RMT model and conformal model. In subsection 4.1, we quickly review the DSSYK model with emphasis on those properties which are relevant to our work. In the remaining part of section 4, we discuss the transport in the DSSYK systems. In section 5, we conclude with some possible future directions.

---

<sup>2</sup>We emphasize here that these numerics are not very intensive unlike simulating the full system in the generic model or solving the Schwinger Dyson equations in the case of SYK model.

## 2 Setup for the heat transport and some toy models

In this section, we describe the setup used to study heat transport in detail. We consider two distinct systems, referred to as the hot and cold systems, initially held at temperatures  $T_c$  and  $T_h$  respectively with  $T_h > T_c$ . These systems are coupled at time  $t = 0$  via operator interaction. The total Hamiltonian is given by<sup>3</sup>

$$\mathcal{H} = H_c + H_h + \theta(t)\epsilon O_c O_h , \quad (2.1)$$

where  $O_c, O_h$  are operators in the cold and the hot system respectively. The entire system evolves under the full Hamiltonian  $\mathcal{H}$  and the energies of the cold and hot system denoted by  $E_c(t), E_h(t)$  change with time. The goal of this section is to establish some general formulae that can be used to compute the heat current  $\dot{E}_c(t) \equiv \frac{dE_c}{dt}$  to leading order in  $\epsilon$ , the strength of the coupling between the systems. In addition, we will derive expressions for the thermal conductivity from the long-time behavior of the heat current  $\dot{E}_c(t)$ .

### 2.1 Description of the isolated quantum system

We begin by describing the properties of individual quantum systems. The Hamiltonian is denoted by  $H$  and we restrict ourselves to systems whose energy spectrum is confined to the interval  $(-E_0, E_0)$  with  $E_0 > 0$ <sup>4</sup>. We assume that the spectrum is symmetric about  $E = 0$ , such that the density of states  $\rho(E)$  satisfies

$$\rho(E) = 0 \quad \forall |E| \geq E_0, \quad \rho(E) = \rho(-E) . \quad (2.2)$$

The partition function of the system at inverse temperature  $\beta$  is given by

$$Z(\beta) \equiv \text{Tr} (e^{-\beta H}) = \int_{-E_0}^{E_0} dE \rho(E) e^{-\beta E} . \quad (2.3)$$

Note that since  $\rho(E)$  is an even function of  $E$ ,  $Z(\beta)$  is an even function of  $\beta$ . The two point function of any operator  $O$  in the system is given by

$$G(t) \equiv \frac{\text{Tr}(O(t) O e^{-\beta H})}{Z(\beta)} = \frac{1}{Z(\beta)} \int \int dE_1 dE_2 \rho(E_1) \rho(E_2) e^{-\beta E_2 + it(E_2 - E_1)} f(E_1, E_2) , \quad (2.4)$$

---

<sup>3</sup>The equation below does not fully capture the setup for the DSSYK systems discussed in section 4, where the coupling  $\epsilon$  also includes disorder. See footnote 24 in Appendix A for details. However, as shown there, the results for the heat current remain identical to those obtained using the simplified form presented here.

<sup>4</sup>In some cases, we will consider the limit  $E_0 \rightarrow \infty$  - see the conformal regime in section 4.2.1

where  $f(E_1, E_2) = \overline{|\langle E_1 | O | E_2 \rangle|^2}$  represents the average over the energy eigen states of the square of matrix element of operator  $O$ . By definition,  $f(E_1, E_2)$  is a positive and symmetric function i.e.,  $f(E_1, E_2) = f(E_2, E_1) > 0$ .

Without loss of generality, we assume that the one-point function of  $O$  vanishes, i.e  $\text{Tr}(Oe^{-\beta H}) = 0$ . In addition, we impose the symmetry  $f(E_1, E_2) = f(-E_1, -E_2)$ , in analogy with the behavior of the density of states. It will also be useful to write the two point function in the frequency domain as <sup>5</sup>

$$\tilde{G}(\omega) = \frac{2\pi e^{\frac{\beta\omega}{2}}}{Z(\beta)} \int_{-E_0+\frac{|\omega|}{2}}^{E_0-\frac{|\omega|}{2}} dE \rho(E + \frac{\omega}{2}) \rho(E - \frac{\omega}{2}) f(E + \frac{\omega}{2}, E - \frac{\omega}{2}) e^{-\beta E} . \quad (2.5)$$

From the above definition, it is clear that  $\tilde{G}(\omega)$  vanishes for  $|\omega| > 2E_0$  since that is the maximum energy the system can absorb. It is useful to note the following properties of the two point function

- **Reality condition:** The two point function satisfies

$$G^*(-t) = G(t), \quad \tilde{G}^*(\omega) = \tilde{G}(\omega) . \quad (2.6)$$

- **KMS relation:** Two point function satisfies the KMS relation

$$G(t) = G(-t - i\beta), \quad \tilde{G}(-\omega) = e^{-\beta\omega} \tilde{G}(\omega) . \quad (2.7)$$

- **Behavior near  $t = 0$ :** We will normalize the two point function so that  $G(t = 0) > 0$  is  $\beta$  independent<sup>6</sup>. Additionally, note that  $\text{Im}\dot{G}(0) < 0$ , since

$$Z(\beta) \text{Im}[\dot{G}(0)] = \int dE_1 dE_2 \rho(E_1) \rho(E_2) [E_2 - E_1] [e^{-\beta E_2} - e^{-\beta E_1}] ,$$

which is explicitly negative.

---

<sup>5</sup>Our convention for Fourier transform is,

$$\tilde{f}(\omega) = \int_{-\infty}^{\infty} dt e^{i\omega t} f(t), \quad f(t) = \int_{-\infty}^{\infty} \frac{d\omega}{2\pi} e^{-i\omega t} \tilde{f}(\omega)$$

<sup>6</sup>This is an unusual choice, but it happens to be true for the DSSYK model as we will see explicitly later

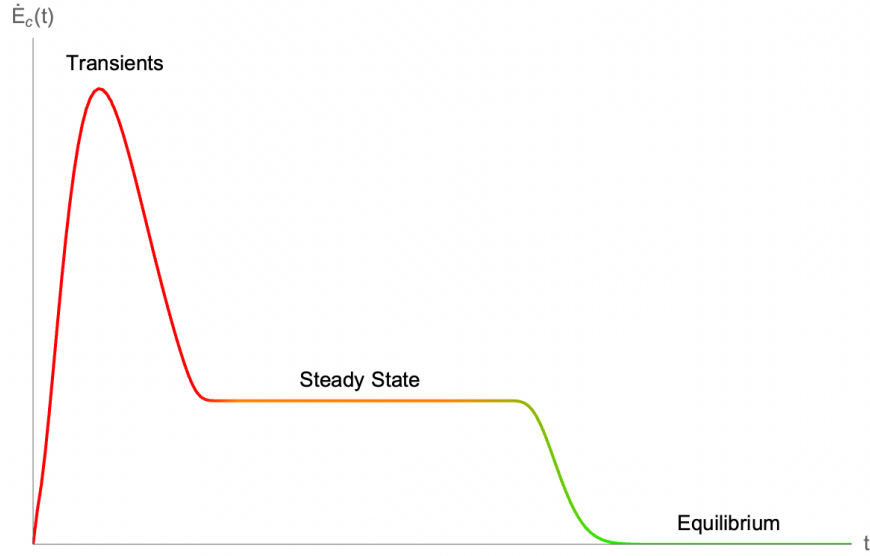


**Figure 3:** Typical heat current when two systems at different temperatures are coupled, adapted from fig(1) of [6]

## 2.2 Heat transport between quantum systems

To study the heat transport, we consider two individual quantum systems as described in the previous subsection, initially held at different temperatures  $T_c$  and  $T_h$  with  $T_c < T_h$  (the subscript refer to cold and hot systems respectively). These systems are coupled at times  $t \geq 0$ , via operator coupling  $O_c O_h$ . The Hamiltonian for  $t > 0$  is given by eq(2.1).

Our goal is to compute the energy change in each of the two systems as a function of time  $t$  to leading order in  $\epsilon$ . The energy current/heat current of the cold system is given by

$$\dot{E}_c(t) \equiv \frac{1}{Z(\beta_c)Z(\beta_h)} \text{Tr} \left[ \dot{H}_c(t) \rho(t=0) \right], \quad \rho(t=0) = e^{-\beta H_c - \beta H_h}. \quad (2.8)$$

Here  $H_c(t)$  denotes the cold system Hamiltonian evolved using the full Hamiltonian  $\mathcal{H}$  given in eq(2.1).

In figure(3), we give a typical expected behavior of the heat current  $\dot{E}_c(t)$  computed this way (see [6] for instance). As shown in the figure, the heat current typically starts from zero, reaches a peak at early times, then decreases and settles to an approximately constant value at intermediate times. This plateau corresponds to a non-equilibrium steady state (NESS). At late times, the heat current eventually vanishes as the whole system thermalizes to an intermediate temperature. If the initial systems are very large, the NESS survives for a very long time.

To leading order in coupling  $\epsilon$ , the heat current can be expressed in terms of the two point function of the operator  $O$  in the isolated quantum system. Denoting the two point function of  $O_c, O_h$  by  $G_c(t), G_h(t)$  respectively (see eq(2.4)), the heat current to leading order in  $\epsilon$  is given by (see Appendix A for a detailed derivation)

$$\dot{E}_c(t) = -\epsilon^2 \text{Im} \{G_c(t)G_h(t)\} + \underbrace{\epsilon^2 \text{Im} \int_0^t d\tilde{t} \left\{ G_c(\tilde{t})\dot{G}_h(\tilde{t}) - \dot{G}_c(\tilde{t})G_h(\tilde{t}) \right\}}_{\equiv \dot{E}_-} . \quad (2.9)$$

Here we have defined the energy current between the systems  $\dot{E}_-(t)$  for use in later discussions. It is useful to note that the first term in the expression for the heat current dominates during the transient regime — i.e., at early times—after which it decays and becomes negligible. At longer times, the second term, namely  $\dot{E}_-$  becomes relevant.

In this work, we compute the heat current for various toy models as well as the DSSYK model focusing on its behavior up to intermediate times where the non-equilibrium steady state (NESS) emerges. Specifically, we will analyze and characterize the following aspects

- **Transients** : At early times, the heat current is sensitive to the details of the quantum systems. In all the models analyzed in this work, we observe a linear increase in heat current (both  $\dot{E}_c(t), \dot{E}_h(t)$ ) at small times, followed by a peak at a characteriztic peak time  $t_p$ , and then an eventual decrease of the heat current to a constant value.<sup>7</sup> This is consistent with findings of [6], where it was also proven that the integrated energy flux

$$F_\kappa \equiv \int_0^\infty dt e^{-\kappa t} \dot{E}_h .$$

obeys the the following inequality

$$F_\kappa \geq 0, \quad \forall \kappa \geq \frac{2}{\beta_h} . \quad (2.10)$$

We verify that this result holds for all the models considered in this work.

The linear rise of  $\dot{E}_c(t)$  at early times can be understood analytically since

$$\dot{E}_c(t) = -2t G_h(0)\text{Im}[\dot{G}_c(0)] + \mathcal{O}(t^2) ,$$

which is manifestly positive since  $G(0) > 0$ ,  $\text{Im}G(0) < 0$ , as noted before.

---

<sup>7</sup>The fall need not be monotonic, there could be oscillations too as we will see.

- **Approach to steady state** : At intermediate times, the two-point functions decay, and the heat current,  $\dot{E}_c$  approaches a positive constant. The nature of this approach depends on the decay profile of the two-point function—whether it be power-law, exponential, or Gaussian. All these behaviors are observed in the models we study. It is useful to note that for systems with long-lived quasiparticles, an exponential decay is typically expected.
- **Steady state** : As mentioned above, at later times, the system settles to a steady state characterized by a constant heat current denoted by  $\dot{E}_c(\infty)$  which can be obtained as the  $t \rightarrow \infty$  limit of eq(2.9) neglecting the first term,<sup>8</sup> which vanishes at large  $t$ . In the Fourier representation, the time integral yields a Dirac delta enforcing  $\tilde{\omega} = -\omega$ , and we obtain

$$\begin{aligned}\dot{E}_c(\infty) &= -\epsilon^2 \int_{-\infty}^{\infty} \frac{d\omega}{2\pi} \omega \tilde{G}_c(\omega) \tilde{G}_h(-\omega) \\ &= -\epsilon^2 \int_0^{\infty} \frac{d\omega}{2\pi} \omega \tilde{G}_c(\omega) \tilde{G}_h(\omega) (e^{-\beta_c \omega} - e^{-\beta_h \omega}) .\end{aligned}\tag{2.11}$$

Here we have used the KMS relation in frequency space eq(2.7).

The above expression captures the steady-state energy flow from the hot system to the cold one, as indicated by the fact that  $\dot{E}_c(\infty) = -\dot{E}_h(\infty)$  and that  $\dot{E}_c(\infty) > 0$ . In the limit where  $T_h$  is very close to  $T_c$ , the heat current satisfies Fourier's law, viz.,

$$\dot{E}_c(\infty) = \sigma(T_h - T_c) + \mathcal{O}(T_h - T_c)^2 ,$$

where  $\sigma$  is the thermal conductivity. This can be computed as

$$\begin{aligned}\sigma &= \epsilon^2 \beta^2 \operatorname{Im} \int_0^{\infty} dt \left( \partial_\beta G(t) \dot{G}(t) - \partial_\beta \dot{G}(t) G(t) \right) \\ &= \epsilon^2 \beta^2 \int_0^{\infty} \frac{d\omega}{2\pi} \omega^2 \tilde{G}(\omega)^2 e^{-\beta \omega} ,\end{aligned}\tag{2.12}$$

where  $\beta$  is the average inverse temperature. In going to the second line, we have used the KMS relation eq(2.7) and linearized the temperature dependence around the average  $\beta$ .

In the next subsections, we analyze three toy models, in which we observe all three key features of heat transport discussed earlier—namely, the transient rise in heat current, the approach to a steady state, and the establishment of a non-equilibrium steady-state (NESS) with a constant heat current.

---

<sup>8</sup>At large enough times, the  $\mathcal{O}(\epsilon)^2$  the approximation we are working with eventually breaks down. Here, by "large times," we mean  $t$  much greater than the decay timescale of the two-point function.

### 3 Heat transport in toy models

In this section, we study the heat transport between two quantum systems as outlined in the previous section when the quantum systems involved are described by certain toy models. In what follows, we introduce three toy models, namely the *Random Matrix Theory model* in subsection 3.1, the *conformal model* in subsection 3.2 and the *gaussian model* in the subsection 3.3<sup>9</sup>. We systematically characterize both the transient dynamics and the steady-state behavior of the heat current.

#### 3.1 Toy Model 1 : Random Matrix Theory (RMT)

In the Random Matrix Theory (RMT) model, the energy spectrum is taken to be the well-known Wigner semicircle law:

$$\rho(E) = \frac{2\mathcal{N}_r \sqrt{E_0^2 - E^2}}{\pi E_0^2} . \quad (3.1)$$

Here  $\mathcal{N}_r$  is a normalization factor, which we will keep arbitrary for now.

Now we move to modeling the matrix element square of a generic operator in the energy basis. The simplest choice is perhaps to take the matrix element square average  $f(E_1, E_2)$  to be a constant independent of the energies  $E_1$  and  $E_2$ . However, we want to allow for a suppression of matrix elements between energetically distant states compared to nearby ones. To this end, we consider a form with a mild energy dependence<sup>10</sup>

$$f(E_1, E_2) = f_0 \left( 1 + \frac{\Delta}{E_0^2} E_1 E_2 \right) , \quad (3.2)$$

for some constants  $f_0, \Delta$  where  $1 > \Delta > -1$  since  $f(E_1, E_2) > 0$ . The above form means that, for positive  $\Delta$ , the average matrix element square  $f(E_1, E_2) < f_0$  when  $E_1$  and  $E_2$  are of opposite sign, i.e., when they are on either side of the maximum energy. When  $E_1$  and  $E_2$  are of the same sign,  $f(E_1, E_2) > f_0$ . The combination  $\frac{1-\Delta}{1+\Delta}$  can then be interpreted as characterizing the suppression of matrix elements between energetically distant states compared to nearby ones. We take the above formulae for  $\rho(E)$  and  $f(E_1, E_2)$  to be the definition of our toy model 1. Phrased this way, our

---

<sup>9</sup>We will see that the gaussian model can be thought of as a special case of conformal model

<sup>10</sup>In general,  $f(E_1, E_2)$  can be expressed as a systematic power series in  $E_1, E_2$  (expanded around say  $E = -E_0$ ) consistent with the symmetries. In fact, for the realistic model of DSSYK as we will see in eq(4.14),  $f(E_1, E_2)$  takes precisely such a form. While the truncated form we use here may or may not appear natural for generic operators in RMT, it is justified in the regime of long times or low temperatures. In these regimes, the dominant contribution to the dynamics arises from states near the ground state (or near the highest excited state, due to symmetry). Truncating to  $\mathcal{O}((E_1 - E_0)(E_2 - E_0))$  and imposing the symmetries results in the expression below.

model depends on only on two dimensionless parameters:  $\beta E_0$  and  $\Delta$  (the parameters  $f_0, \mathcal{N}_r$  appear only as overall factors).

The above model may seem somewhat crude and ad hoc - after all, we are not giving some detailed picture of where the underlying spectrum and matrix elements come from. But, as will be seen momentarily, this already captures lot physics behind both the heat transients as well as of approach to NESS. The very simplicity of the model allows us to do exact computations. Furthermore, as we shall see, in an appropriate regime, DSSYK model reduces to this model, thus giving a concrete realization in terms of disordered fermions.

The partition function eq(2.3) can be calculated analytically and is given by

$$Z(\beta) = \frac{2\mathcal{N}_r I_1(\beta E_0)}{\beta E_0} ,$$

where  $I_1$  is the modified Bessel function of the first kind. It will be convenient to define the quantity

$$\tilde{Z}(\beta) \equiv -\frac{1}{E_0} \int_{-E_0}^{E_0} dE \rho(E) e^{-\beta E} E = \frac{2\mathcal{N}_r I_2(\beta E_0)}{\beta E_0} , \quad (3.3)$$

which is the (negative of the) internal energy of the system in  $E_0$  units. For the two point function, we get from eq(2.4) the following result:

$$G(t) = f_0 \frac{Z(it)Z(\beta - it)}{Z(\beta)} + f_0 \Delta \frac{\tilde{Z}(it)\tilde{Z}(\beta - it)}{Z(\beta)} . \quad (3.4)$$

In figure(4), we plot the the heat current  $\dot{E}_c(t)$  at two different temperatures, computed using eq(2.9). The plot clearly displays both the transient regime at early times and the emergence of a steady-state regime at intermediate times. In the following discussion, we provide a detailed characterization of these two regimes.

**Transients** To characterize the transient behavior, we identify the peak time  $t_p$  —the time at which the heat current  $\dot{E}_c(t)$  reaches its maximum.

- As shown in figure(5),  $t_p$  is observed to be largely independent of  $\beta$ , regardless of the value of  $\Delta$ .
- In figure(6), we also plot the peak height  $\dot{E}_c(t_p)$  as a function of  $\beta$ . This plot shows how the magnitude of the initial energy surge depends on temperature: we see the peak height vary linearly with  $\beta$  at high temperatures. At low temperatures, the peak height is pretty much independent of temperature.
- The integrated energy flux  $F_\kappa$  is positive for all  $\kappa \geq \frac{2}{\beta_h}$  as can be seen in figure(7).

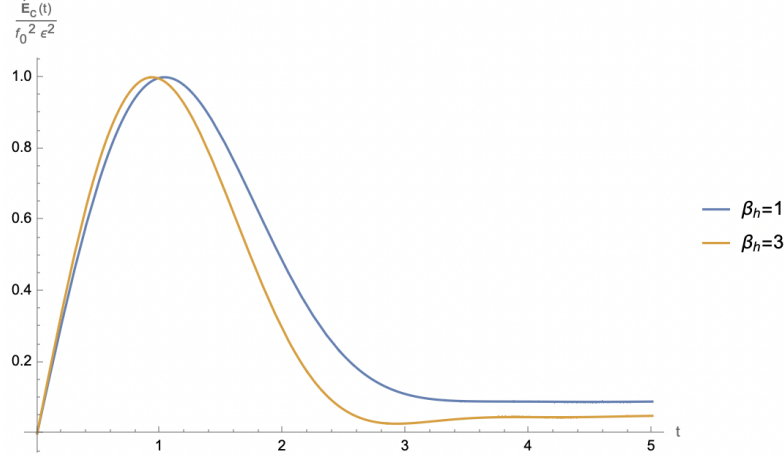


**Figure 4:** behavior of heat current for systems at different temperatures with  $\Delta = 0.1$ ,  $E_0 = 1$ ,  $\beta_c = 1.1\beta_h$ ,  $\mathcal{N}_r = 1$ , normalized so that peak height is 1

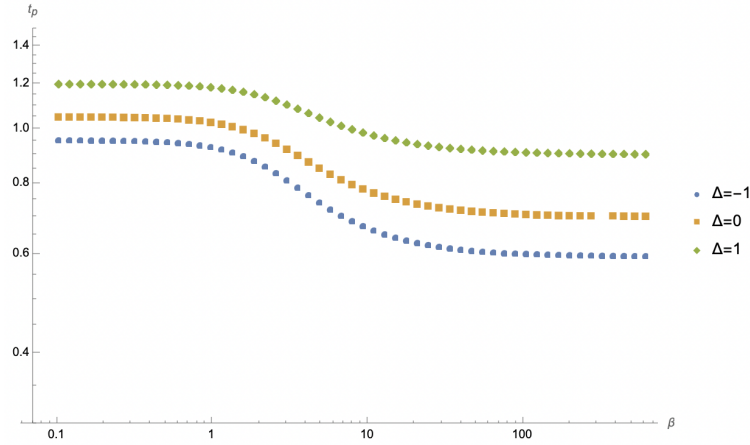


**Figure 5:** Peak time vs temperatures for systems with  $E_0 = 1$ ,  $\beta_c = 1.1\beta_h$  and different values of  $\Delta$ .

**Approach to the steady state and thermal conductivity** Given the formulae given earlier, we can easily analyze the long-time behavior of the heat current using Bessel asymptotics. In the limit  $tE_0 \gg 1$  (with no restrictions on  $\beta$ ), the two-point function given in eq(3.4) simplifies considerably using the asymptotic form of Bessel functions (see appendix B.1 for details). We get

$$G(t) = \frac{4(1-\Delta)f_0\mathcal{N}_r^2}{\pi E_0^3 Z(\beta)} \frac{\left[ \frac{1+\Delta}{1-\Delta} \cosh(\beta E_0) - \sin(2E_0 t + i\beta E_0) \right]}{[t(t+i\beta)]^{\frac{3}{2}}} \left[ 1 + \mathcal{O}((t^2 + \beta^2)^{-\frac{1}{2}}) \right]. \quad (3.5)$$

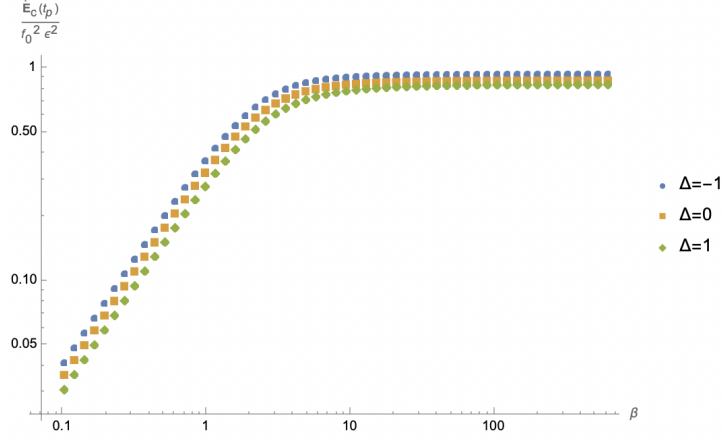


**Figure 6:** Peak height vs temperatures for systems with  $E_0 = 1$ ,  $\beta_c = 1.1\beta_h$ ,  $\mathcal{N}_r = 1$  and different values of  $\Delta$ . The peak height fits to  $a\beta$  for small  $\beta$  with the slope  $a$  values  $\{0.31, 0.28, 0.24\}$  corresponding to  $\Delta$  values  $\{-1, 0, 1\}$ .

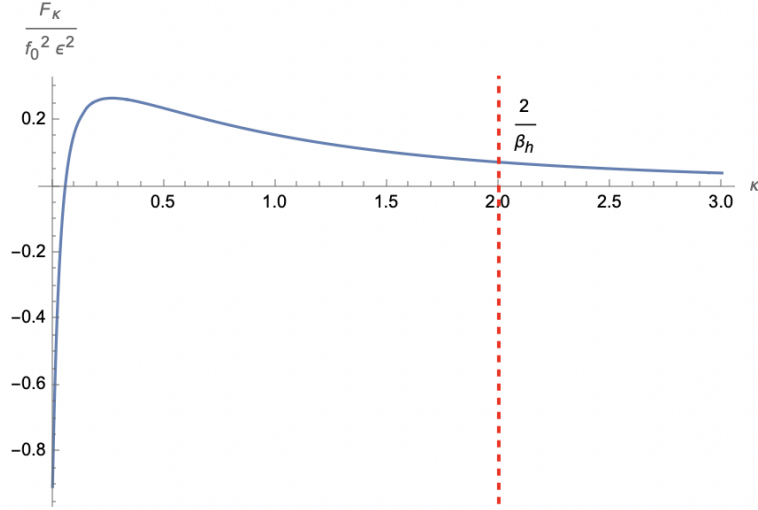


**Figure 7:**  $F_\kappa$  vs  $\kappa$  for a sytem with  $E_0 = 1$ ,  $\beta_c = 1.1$ ,  $\beta_h = 1$ ,  $\Delta = 0.1$ ,  $\mathcal{N}_r = 1$ .

This is an interesting expression exhibiting power law at late times, modulated by oscillations. We also see that the parameter  $1 - \Delta$  governs the oscillatory behavior in time.

Substituting the above result into the heat current expression given in eq(2.9) we

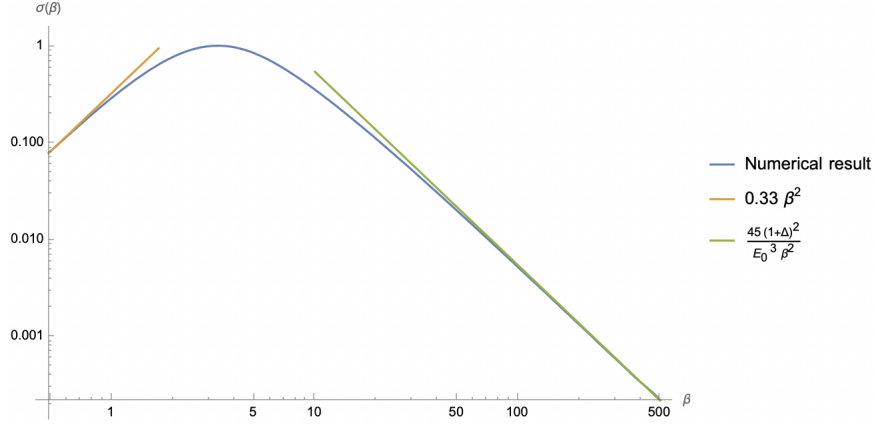


**Figure 8:** Conductivity as a function of  $\beta$  for  $E_0 = 1$ ,  $\Delta = 0.1$ ,  $\mathcal{N}_r = 1$ .

have the following asymptotic form<sup>11</sup>

$$\begin{aligned} \dot{E}_c(t) = \dot{E}_c(\infty) - \frac{32f_0^2\mathcal{N}_r^4(1-\Delta)^2}{\pi^2 Z(\beta_c)Z(\beta_h)(E_0 t)^5} & \left[ \frac{\sinh(E_0(\beta_c - \beta_h))}{5} \right. \\ & + \frac{\sin(4E_0 t) \sinh(E_0(\beta_c + \beta_h)) - 4\frac{1+\Delta}{1-\Delta} \cos(2E_0 t) \sinh(E_0\beta_c) \cosh(E_0\beta_h)}{4E_0 t} \Big] \\ & + \mathcal{O}(t^{-7}) . \end{aligned} \quad (3.6)$$

We thus observe a power law  $1/t^5$  type approach to the steady state. Given the simplicity of this derivation, we suspect that this power law approach to steady state is universal across a large class of models which look like random matrix theory.

Finally, we turn to the steady state itself: the conductivity eq(2.12) can be numerically evaluated and the result is shown in figure(8). As seen in the plot, the conductivity exhibits power-law fall off at both the high- and low-temperature regimes, and it shows a maxima at an intermediate temperature. The low-temperature (i.e., large  $\beta$ ) scaling seen in the figure can be understood via a low-temperature analysis, to be outlined in the subsection 3.1.1 (See eq(3.11)).

We will now like to explore whether even simpler effective models can capture the physics of the RMT model in the long-time, low-temperature regime. In this limit, we expect the two-point function—and consequently, the heat current to be governed by the singularities in the density of states  $\rho(E)$ , and the matrix element averages

<sup>11</sup>Interestingly, for the case  $\Delta = 1$  case, the leading contribution to the heat current vanishes, and the behavior of  $\dot{E}_c(t)$  is suppressed as  $\mathcal{O}(t^{-7})$  at long times.

$f(E_1, E_2)$ , in the vicinity of these singularities. Since the edges of the density of states exhibit a square-root dependence on energy i.e.,  $\rho(E) \propto \sqrt{E - E_0}$ , it is natural to ask whether this feature alone is sufficient to reproduce the observed RMT model behavior. In the next subsection, [3.1.1](#), we answer this question affirmatively.

We introduce in next subsection a simplified model, which we refer to as *Cold RMT model*, that retains only the relevant features near the edge of the spectrum, and allows for explicit analytic expressions for the long time observables like conductivity and approach to NESS regimes. This toy model is particularly relevant to the DSSYK model since, as we will see later, at sufficiently low temperatures and long times (for  $\beta, t \gg (1 - q)^{-\frac{3}{2}}$ ), DSSYK also reduces to the Cold RMT model.

### 3.1.1 Cold Random Matrix Theory

In this subsection, we introduce the Cold Random Matrix Theory (Cold RMT) model which effectively captures the long time low temperature behavior of the RMT model described in the previous section [3.1](#). As noted earlier, near the lower edge of the spectrum (i.e., close to the ground state), the RMT density of states takes the form

$$\rho(E) = \frac{2\sqrt{2}\mathcal{N}_r}{\pi E_0^{\frac{3}{2}}} \sqrt{E_0 + E} .$$

While we could work with just this model, we consider slightly more general class of models parametrized by  $\alpha$  to capture the effect of singularity structure of density of states as follows

$$\rho(E) = \frac{\sqrt{2}\mathcal{N}_r}{\sqrt{\pi}\Gamma(1 + \alpha)E_0^{\alpha+1}} (E_0 - |E|)^\alpha, \quad |E| < E_0 , \quad (3.7)$$

for some constants  $\alpha > 0$ . The model above matches the RMT model near the edges for  $\alpha = \frac{1}{2}$ . We are interested in the long time low temperature limit of this model where the results are expected to match RMT model results for  $\alpha = \frac{1}{2}$ . The partition function at low temperatures, i.e., large  $\beta E_0$  becomes

$$Z(\beta) \approx \frac{\sqrt{2}\mathcal{N}_r e^{\beta E_0}}{\sqrt{\pi}(\beta E_0)^{\alpha+1}} . \quad (3.8)$$

- The partition function of the RMT model at low temperatures (i.e., large  $\beta E_0$ ), agrees with the above result for  $\alpha = \frac{1}{2}$ , confirming that the Cold RMT correctly captures the low temperature physics of RMT (this also justifies the name).
- Further, in the low temperature, long time limit of the two point function in the cold RMT matches the result in the RMT case given in [eq\(3.5\)](#).

- This in turn implies that the power law approach of the heat current to its NESS in the cold RMT case is  $t^{-4\alpha-3}$  which for the  $\alpha = \frac{1}{2}$  is  $t^{-5}$  which is the same as the RMT case seen before in eq(3.6).

We now turn to obtaining analytical expression for conductivity in the cold RMT model. To do this, we first evaluate the two-point function in frequency space using eq(2.5) in the low-temperature limit. By extending the upper limit of the time integral to  $\infty$ , valid for  $\beta E_0 \gg 1$ , we obtain:

$$\tilde{G}(\omega) \approx \frac{2\sqrt{2}f\mathcal{N}_r(1+\Delta)}{E_0\Gamma(\alpha+1)} e^{\frac{\beta\omega}{2}} (|\omega|/E_0)^\alpha \sqrt{\beta|\omega|} K_{\alpha+\frac{1}{2}}\left(\frac{\beta|\omega|}{2}\right), \quad (3.9)$$

where we have kept  $\omega\beta$  fixed. The resulting expression explicitly satisfies KMS. We can obtain conductivity from eq(2.12)

$$\sigma \approx \frac{2^{2\alpha+3}\epsilon^2\mathcal{N}_r^2f_0^2(1+\Delta)^2}{E_0} \frac{(\alpha+1)\Gamma(2\alpha+\frac{5}{2})}{\Gamma(\alpha+1)\Gamma(\alpha+\frac{5}{2})} (\beta E_0)^{-1-2\alpha}. \quad (3.10)$$

For  $\alpha = \frac{1}{2}$  we get,

$$\sigma = \frac{45\epsilon^2f_0^2\mathcal{N}_r^2(1+\Delta)^2}{E_0^3\beta^2}. \quad (3.11)$$

This is consistent with low temperature features seen before in figure(8). This line of analysis shows how the low temperature power laws in RMT model directly follow from the behavior of the spectrum near the edges.

### 3.2 Toy Model 2 : Conformal model

We will now describe a second toy model for heat transport which exhibits a qualitatively different behavior than the RMT model above. We will see later that, like the RMT model, this model can also be realized as a limit of DSSYK in an appropriate regime.

We will call this second model as *conformal model*, since it captures features of conformal quantum mechanical systems at finite temperature. The conformal regime is characterized by the zero temperature two point function  $G(t)$  scaling as  $t^{-2m}$  for some exponent  $m$ . The corresponding finite temperature result can then be obtained by a simple conformal transformation. This motivates a finite temperature two point Wightman function of the form

$$G(t) \sim \sinh^{-2m}\left(\frac{\pi(t-i\delta)}{\beta}\right), \quad (3.12)$$

where  $m, \delta$  are some parameters. Here  $\delta$  is a UV cutoff which regulates the conformal behavior for small times  $t \ll \delta$ .

A two point function of the above form arises for instance in the low temperature limit of SYK models, in an emergent scale invariant regime[52]. The exponent  $m$  is related to the conformal dimension of the operator in the IR, whereas  $\delta$  models the sensible UV behavior that cuts off the conformal regime in this model. In the SYK model  $\delta$  is fixed by UV physics - see [35] for corresponding analytical statements and [6] for numerical results. We will see in the next section that, in the DSSYK model as well, an analogous SYK-like limit leads to a finite value of  $\delta$ .<sup>12</sup>

We would like a two point function of the above form that also obeys the KMS condition  $G(t) = G(-t - i\beta)$  (which the above form does not as it currently stands). This is achieved by the following ansatz for the two point function

$$G(t) = \frac{f_0 \sinh^{2m}(-i\theta_0)}{\sinh^{2m}(\frac{2\phi_0 t}{\beta} - i\theta_0)}, \quad (3.13)$$

where  $f_0$  is some overall normalization,  $m$  is the scaling exponent, and  $\phi_0$  and  $\theta_0$  are parameters related by  $\theta_0 + \phi_0 = \frac{\pi}{2}$  so that KMS is preserved. In some cases, it is convenient to make the KMS condition explicit by expressing  $\theta_0$  in terms of  $\phi_0$ , yielding:

$$G(t) = \frac{f_0 \cos^{2m}(\phi_0)}{\cos^{2m}(\frac{\phi_0}{\beta}(\beta - 2it))}. \quad (3.14)$$

Note that, in specifying the conformal model, we have not described the density of states  $\rho(E)$  and the averaged squared matrix element of operators  $f(E_1, E_2)$  as we did for the RMT model. Rather we find it convenient to directly write down the two point function which is after all what is needed to study heat transport.<sup>13</sup>

Having specified the model via the above two point function, let us move to describe its consequences. One striking difference between the RMT vs. the conformal models is their large time behavior. At large times, the two-point function of conformal model exhibits exponential decay, i.e.,

$$G(t) = f_0 \left(2e^{-i\phi_0} \cos \phi_0\right)^{2m} e^{-\frac{4mt\phi_0}{\beta}},$$

---

<sup>12</sup>For instance, in frequency space, DSSYK two point function is given in eq(C.8) where  $\phi_0$  is related to  $\delta$  via  $\phi_0 = \frac{\pi}{2} - \delta$ .

<sup>13</sup>We will see later two cases where we get explicit expressions for  $\rho(E), f(E_1, E_2)$  which can give rise to such a two point function. First one is the Gaussian model in subsection 3.3, which can be thought of as a heavy operator (i.e.,  $m \gg 1$ ) limit of the conformal model. The second instance is a specific conformal regime of DSSYK (see section 4.2.1).

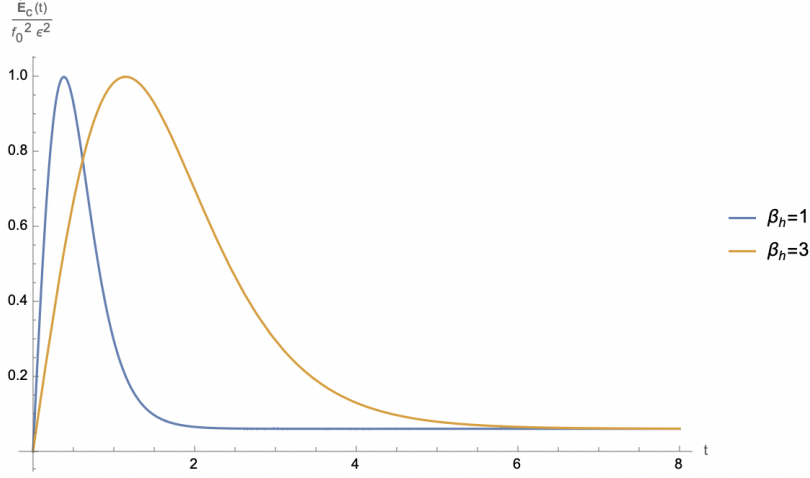


**Figure 9:** Behavior of  $\dot{E}_c$  for systems at different temperatures,  $\theta_0 = \frac{\pi}{3}$  and  $m = 1$ ,  $\phi_0 = \frac{\pi}{6}$  with peak heights normalized to 1.

in sharp contrast to the power-law falloff seen in the RMT models. The two point function in frequency domain can be determined to be<sup>14</sup>,

$$\tilde{G}(\omega) = \frac{f_0 \beta}{4\phi_0} \frac{(2 \cos \phi_0)^{2m}}{\Gamma(2m)} e^{\frac{\beta \omega}{2}} \Gamma\left(m + \frac{i\beta \omega}{4\phi_0}\right) \Gamma\left(m - \frac{i\beta \omega}{4\phi_0}\right) \quad (3.15)$$

The function  $\tilde{G}(\omega)$  has isolated poles at  $\beta \omega = \pm 4i(m+n)\phi_0$ ,  $\forall n \geq 0$ . For the SYK models at low temperatures, these quasinormal modes were observed in [54]. This should be contrasted with the case of Cold RMT where  $\tilde{G}(\omega)$  had branch cut singularities at least at low temperatures - see eq(3.9). This difference is perhaps one reason why the large time asymptotics are so different in these two models.

We can compute the heat current by plugging the above expressions into eq(2.9) and plot  $\dot{E}_c(t)$  in the figure(9) for two different temperatures. The plot clearly shows all the three features : transients, approach to steady state and steady state.

---

<sup>14</sup>We have used the result [53]

$$2^{2m} \int_{-\infty}^{\infty} \frac{d\omega}{2\pi} e^{-i\tau\omega} \frac{\Gamma(m+i\omega)\Gamma(m-i\omega)}{\Gamma(2m)} = \cosh^{-2m} \frac{\tau}{2}, \quad \text{Re}(m) > 0.$$

Note that since  $\lim_{\omega \rightarrow \pm\infty} \Gamma(m+i\omega)\Gamma(m-i\omega) = 2\pi|\omega|^{2m-1}e^{-\pi|\omega|}$ , the integral converges for  $-\pi < \text{Im}(\tau) < \pi$ . The result in the main text follows by setting  $\tau = \frac{4\phi_0 t}{\beta} + 2i\phi_0$ . The convergence criterion then translates to the condition  $-\frac{\pi}{2} < \phi_0 < \frac{\pi}{2}$ .

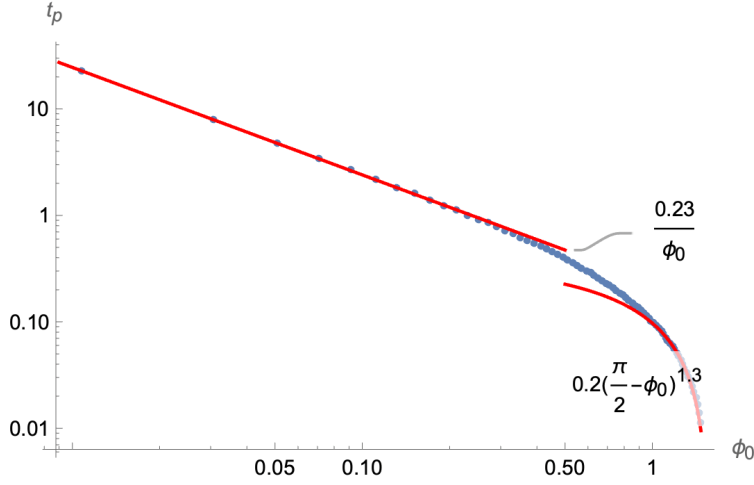


**Figure 10:** Peak time as a function of  $\phi_0$  for conformal model with parameters  $m = 1$ ,  $\beta_c = 1.1\beta_h$  in  $\beta_h = 1$  units.

**Transients:** As in the RMT model, we see a heat surge with a peak. However, the scaling of peak times  $t_p$  and peak height are qualitatively different. We give below the peak position  $t_p$  and peak height for typical values of parameters  $\beta_c, \beta_h, m$  as a function of  $\phi_0$  in figures (10,11). We see that the peak in the heat current occurs earlier and earlier as we increase the parameter  $\phi_0$ , with  $t_p$  scaling inversely with  $\phi_0$  for small  $\phi_0$ . As to the peak height, it grows linearly with  $\phi_0$  and saturates eventually to a constant value as  $\phi_0 \rightarrow \frac{\pi}{2}$ . To summarize, we get smaller and earlier peaks at small  $\phi_0$  whereas larger  $\phi_0$ s result in larger peaks, occurring later. The integrated energy flux  $F_\kappa$  is positive for all  $\kappa \geq \frac{2}{\beta_h}$  as can be seen in figure(12).

**Approach to steady state:** At long times, as we mentioned before  $G(t) \sim e^{-\frac{4\phi_0 t m}{\beta}}$  and the long time behavior of heat current can be computed to be<sup>15</sup>,

$$\dot{E}_c(t) - \dot{E}_c(\infty) \propto e^{-4\phi_0 t m (\beta_c^{-1} + \beta_h^{-1})}. \quad (3.16)$$

In contrast to the RMT results eq(3.6) where we saw a power law approach, here we see an exponential approach to the steady state.

**Steady state:** The conductivity can be calculated using the two point function eq(3.15) as,

$$\sigma = c_m f_0^2 \epsilon^2 \phi_0 \beta \cos^{4m}(\phi_0), \quad (3.17)$$

<sup>15</sup>up to factors which are time independent, but depending on  $\phi_0, m, \beta$ .

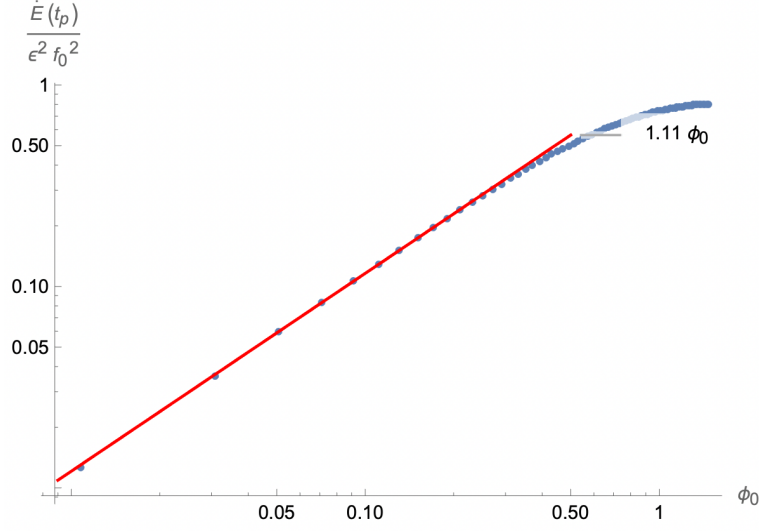


**Figure 11:** Peak height as a function of  $\phi_0$  for conformal model with parameters  $m = 1$ ,  $\beta_c = 1.1\beta_h$  in  $\beta_h = 1$  units.

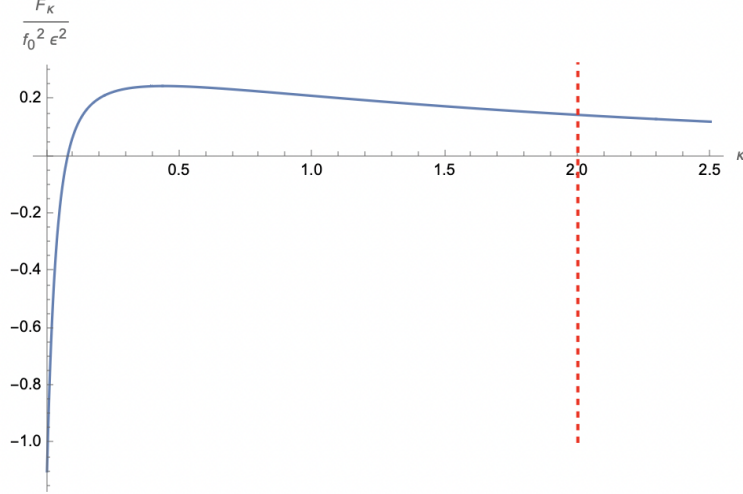


**Figure 12:**  $F_\kappa$  for system at  $\beta_h = 0.1$ ,  $\beta_c = 0.11$  and  $\phi_0 = \frac{\pi}{6}$ ,  $m = 1$

where  $c_m \equiv \frac{2^{4m+1}}{\pi\Gamma(2m)^2} \int_0^\infty d\omega \omega^2 |\Gamma(m+i\omega)|^4 = 2\sqrt{\pi}m^2 \frac{\Gamma(2m)}{\Gamma(2m+\frac{3}{2})}$ . For a fixed  $\phi_0$ , we see that the conductivity varies linearly with  $\beta$ . At a fixed temperature,  $\sigma$  exhibits a maximum at an intermediate  $\phi_0$ .

As a brief aside, we present the expression for thermal conductivity in a more general scenario where the coupled operators  $O_c$  and  $O_h$  (see eq(2.1)) have different scaling dimensions, denoted by  $m_c$  and  $m_h$ . In this case, the thermal conductivity

takes the form

$$\sigma = \frac{\epsilon^2 \beta^2}{2\pi} \int_0^\infty G_c(\omega) G_h(\omega) e^{-\beta \omega} \omega^2 d\omega = c_{m_c, m_h} \epsilon^2 f_0^2 \beta \phi_0 (\cos \phi_0)^{2m_c + 2m_h}, \quad (3.18)$$

where we have defined the prefactor

$$c_{m_c, m_h} \equiv 2^{2m_c + 2m_h + 1} \int_0^\infty \frac{d\omega}{\pi} \omega^2 \frac{|\Gamma(m_c + i\omega)|^2 |\Gamma(m_h + i\omega)|^2}{\Gamma(2m_c) \Gamma(2m_h)}.$$

**Heavy operator limit** There is a special limit in which the conformal toy model results are particularly simple. In the limit of heavy operator,  $m \rightarrow \infty$ ,  $\phi_0 \rightarrow 0$  limit, with the parameter  $J_e \equiv \frac{2\phi_0 \sqrt{m}}{\beta}$  held fixed, the two point function given in eq(3.14) becomes

$$G(t) = f_0 e^{-t(t+i\beta)J_e^2}. \quad (3.19)$$

As we describe in the next subsection, such a two point function can arise from another class of toy models which we term *gaussian models*.

### 3.3 Toy Model 3 : Gaussian model

We will now describe a third simple toy model for heat transport. As indicated before, this model can be thought of as a limit of conformal model, but we think it worthwhile to give the third model an independent description ab initio.

Consider then the *gaussian model* with a density of states

$$\rho(E) = \frac{1}{J\sqrt{2\pi}} e^{-\frac{E^2}{2J^2}}.$$

Here  $J$  sets the energy scale within which most states occur. For example, we expect such a density of states if our system is made of many identical, non-interacting subsystems each having a somewhat random spectrum. By central limit theorem, the distribution of the total energy automatically takes the above form.

The partition function corresponding to the above density of states is also a Gaussian given by

$$Z(\beta) = e^{\frac{\beta^2 J^2}{2}}.$$

We take the averaged squared operator matrix elements to also have a Gaussian dependence on energies, i.e.,

$$f(E_1, E_2) = \frac{f_0}{\sqrt{1 - \tilde{q}^2}} e^{\frac{\tilde{q}}{2(1 - \tilde{q}^2)J^2} [2E_1 E_2 - \tilde{q}(E_1^2 + E_2^2)]}. \quad (3.20)$$

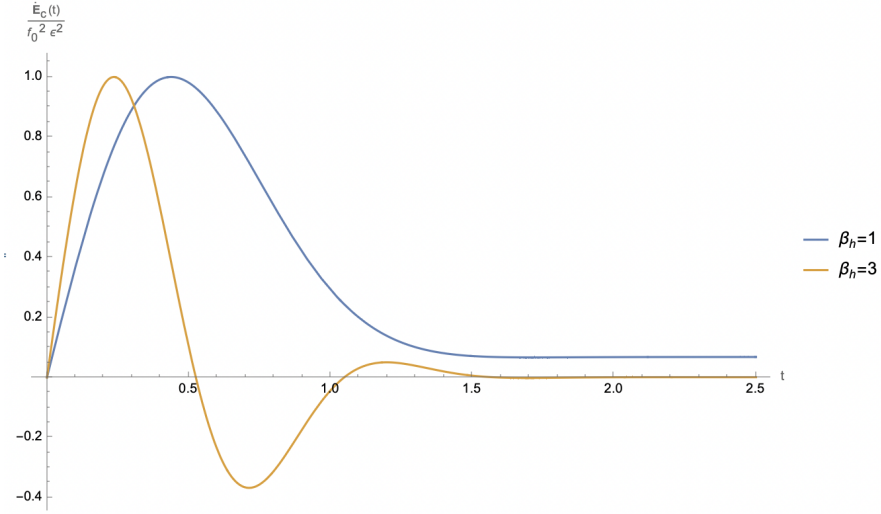


**Figure 13:** behavior of heat current for systems with  $J_e = 1$ ,  $\Delta = 0.1$ . The peak heights are normalized to 1.

Here  $f_0$  is an overall normalization constant. We have also introduced another dimensionless parameter  $\tilde{q}$  in a way that is convenient for computations below. The two point function can be obtained from eq(2.4) to be

$$G(t) = f_0 e^{-t(t+i\beta)J^2(1-\tilde{q})} . \quad (3.21)$$

We note that this exactly matches the heavy operator limit of the conformal toy model given in eq(3.19) with  $J_e \equiv J\sqrt{1-\tilde{q}}$ . The Fourier transform is then given by another Gaussian

$$\tilde{G}(\omega) = \frac{\sqrt{\pi} f_0}{J_e} e^{-\frac{1}{4}\{\beta J_e - \frac{\omega}{J_e}\}^2} . \quad (3.22)$$

This result can also be understood as a limiting case of the conformal model's frequency-space two-point function  $\tilde{G}(\omega)$  eq(3.15) using the asymptotic behavior of the  $\Gamma$  function.

Now that we have the two point function, we can compute the heat current eq(2.9) for this model - the result is plotted in figure(13). We see the same qualitative behavior as the other two models: a heat surge and an approach to steady state. Given that all the integrals involved are Gaussian, many exact analytical expressions can be obtained.

**Transients:** We find the peak time  $t_p$  by solving a transcendental equation

$$\frac{2t_p}{\beta_c} \tan[t_p J_e^2(\beta_c + \beta_h)] = 1 . \quad (3.23)$$

This maps the  $t_p$  computation to computing ground state energy in a finite square well potential (and the subsequent peaks/troughs amount to computing the higher excited

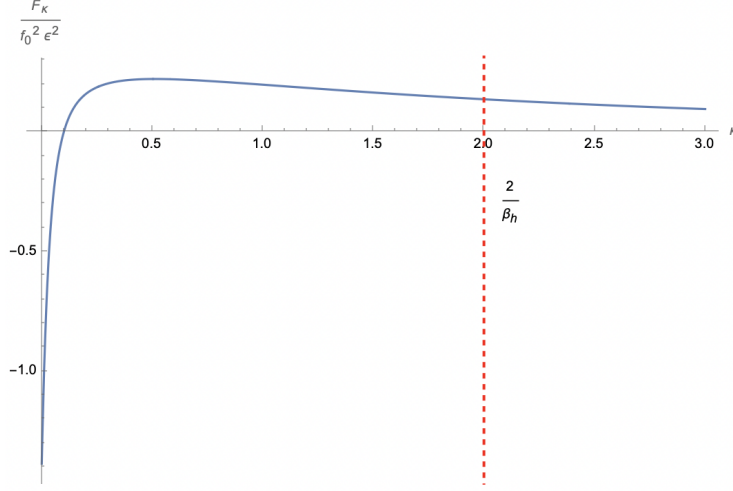


**Figure 14:**  $F_\kappa$  for Gaussian model with  $J_e = 1$

states of even parity in the well). The answer to the finite square well problem is well-known: as the well becomes broader, the ground state energy goes down. Here, similarly, we see that, at a fixed temperature, the heat peak moves to earlier times as we increase  $J_e$ . In the well problem, we get more bound states as the well gets deeper: here we find more peaks and troughs as  $\beta$  increases. Additionally, the integrated energy flux  $F_\kappa$  is positive for all  $\kappa \geq \frac{2}{\beta_h}$  as illustrated in fig(14).

**Approach to Steady state:** We can also explicitly compute the approach to the steady state at large times in this model. In this limit, we obtain

$$\begin{aligned} \frac{\dot{E}_c(t)}{\epsilon^2 f_0^2} = & e^{-2t^2 J_e^2} \sin(t J_e^2 (\beta_c + \beta_h)) \\ & + \frac{(\beta_c - \beta_h)}{4} \left( \sqrt{2\pi} J_e e^{-\frac{J_e^2 (\beta_c + \beta_h)^2}{8}} - \frac{e^{-2t^2 J_e^2} \cos(t(\beta_c + \beta_h) J_e^2)}{t} [1 + \mathcal{O}(t^{-1})] \right). \end{aligned} \quad (3.24)$$

What we see here is that the steady state is reached very quickly governed by a gaussian falloff in time. We see that this is even more faster approach to steady state than the exponential approach in the conformal model, and is in stark contrast to power law approach in the RMT model.

**Steady state:** It is also equally straightforward to characterize the steady state in this model. Using eq(2.12), we can evaluate the conductivity to be,

$$\sigma = \sqrt{\frac{\pi}{2}} \frac{\epsilon^2 \beta^2 f_0^2 J_e}{4} e^{-\frac{\beta^2 J_e^2}{2}}. \quad (3.25)$$

Note that for a fixed  $J_e$ , conductivity falls off both at small and large temperature, with a maximum at some intermediate temperature.

## 4 Heat transport in DSSYK model

In the previous section, we looked at heat transfer in a variety of toy models. encountering broad similarities but also many qualitative differences. The models were simple, but to some extent pulled out of the hat: we never wrote down an explicit Hamiltonian to solve. We would now like to fix this by formulating a full microscopic model which can be solved. It would also be nice to have a single model realise all the behaviors we described in the last section so that we can see what kind of microscopic regimes lead to different kind of heat transfers, To this end, we now move on to the more realistic case of the transport in the Double Scaled Sachdev Ye Kitaev (DSSYK) models.

As in the case of our toy models, the input we need from the DSSYK model to compute the transport is the two point function. Hence we begin in section 4.1 where we quickly summarize the relevant results of DSSYK model. In section 4.2 identify the regimes where the DSSYK model simplifies and reduces to one of the toy models described in the previous section. Finally, we turn to the question of addressing the transport in the DSSYK models in section 4.3.

### 4.1 Review of the double scaled SYK Model

The SYK model [17–19] is a quantum mechanical model of  $N$  fermions with disordered interactions. The Hamiltonian is given by

$$H = \sum_I i^{\frac{p}{2}} J_I X_I. \quad (4.1)$$

Here  $I$  denotes the ordered index set  $\{i_1, i_2, \dots, i_p\}$  (with  $i_1 < i_2 < \dots < i_N$ ) where each of the indices  $i_k \in \{1, \dots, N\}$ ,  $X_I$  denotes a fermion product  $X_I = \chi_{i_1} \dots \chi_{i_p}$  and  $p$  is even. Here  $\chi_i$  are Majorana fermions satisfying  $\{\chi_i, \chi_j\} = 2\delta_{ij}$ . The couplings  $J_I$  are disorder and are taken from an ensemble satisfying

$$\langle\langle J_I J_J \rangle\rangle = \frac{\delta_{IJ}}{\binom{N}{p}} J^2. \quad (4.2)$$

Here  $\langle\langle \dots \rangle\rangle$  denotes disorder averaging, and  $J$  has dimensions of energy. We will mostly work in the units where  $J = 1$  (except in section 4.1.1 where we will temporarily restore  $J$ ). We sometimes refer to the model eq(4.1) as SYK $_p$  model since there are  $p$  fermion interaction in the Hamiltonian.

The double scaling limit of the SYK model [37–40] is defined as the large  $N$  limit, and  $p$  scaling with  $N$  as  $p \propto \sqrt{N}$ . More precisely, double scaling limit is defined via

$$q \equiv e^{-\lambda}, \quad \lambda \equiv \frac{p^2}{N}, \quad \text{held fixed as } N \rightarrow \infty, \quad (4.3)$$

where we have defined a parameter  $q$  with  $0 \leq q \leq 1$ .

The operators of interest in this model are again fermion products, analogous to the ones that appear in the Hamiltonian but with  $\tilde{p}$  number of fermions. We hence define  $O \equiv i^{\frac{\tilde{p}}{2}} \tilde{J}_{\tilde{I}} X_{\tilde{I}}$ , where  $\tilde{I}$  is an ordered index set  $\{i_1, i_2, \dots, i_{\tilde{p}}\}$  and  $X_{\tilde{I}}$  denotes a fermion product  $X_{\tilde{I}} = \chi_{i_1} \dots \chi_{i_{\tilde{p}}}$ .  $\tilde{J}_{\tilde{I}}$  is disorder (independent of  $J_I$  introduced in eq(4.1)) satisfying

$$\langle\langle \tilde{J}_{\tilde{I}} \tilde{J}_{\tilde{K}} \rangle\rangle = \frac{\delta_{\tilde{I}\tilde{K}}}{\binom{N}{\tilde{p}}} \tilde{J}^2.$$

We will normalize the operators such that  $\tilde{J} = 1$ . The double scaled limit of operators are defined as

$$\tilde{q} \equiv e^{-m\lambda}, \quad m = \frac{\tilde{p}}{p}, \quad \text{held fixed as } N \rightarrow \infty. \quad (4.4)$$

Here we have defined another parameter  $\tilde{q}$  with  $0 \leq \tilde{q} \leq 1$ . Throughout this work, we will take the strict  $N \rightarrow \infty$  limit and neglect all  $1/N$  corrections. To summarize, in the double scaling limit, we get the DSSYK model parametrized by  $\lambda, m$  or equivalently  $q, \tilde{q}$ .

In the so called triple scaling limit  $\lambda \rightarrow 0$ , with low temperatures  $\beta \sim \lambda^{-\frac{3}{2}}$ , the familiar SYK physics governed by the Schwarzian action is recovered [38]. The advantage of DSSYK is that we not only have an extra tunable  $\lambda$ , but also the ability to obtain closed-form expressions for several observables across *all energy scales* — not just in the low-energy regime as in the solution of original SYK model.

The relevant object of interest for us in this work are the partition function and the two point function defined as follows

$$Z(\beta) \equiv \langle\langle \text{Tr} (e^{-\beta H}) \rangle\rangle, \quad (4.5)$$

$$G(t) \equiv \frac{1}{Z(\beta)} \langle\langle \text{Tr} (O(t) O e^{-\beta H}) \rangle\rangle. \quad (4.6)$$

Here the trace is normalized such that  $\text{Tr}(\mathbb{I}) = 1$ . Using combinatorial techniques, these observables can be reformulated as sums over chord diagrams [39], which in turn can be recast in terms of a transfer matrix. The contributions at each order can be explicitly written down, and resummed to yield closed form expressions, Our goal here is not to explain all the steps involved which are well-described in the original references. Instead, we will be content with a brief review with results relevant to our problem.

**Partition function**  $Z(\beta)$  The partition function can be reconstructed from the disorder averaged moments of the Hamiltonian  $\langle\langle\text{Tr}H^k\rangle\rangle$ . For the moments, we have that

$$\langle\langle\text{Tr}H^k\rangle\rangle = i^{\frac{kp}{2}} \sum_{I_1, \dots, I_k} \langle\langle J_{I_1} \dots J_{I_k} \rangle\rangle \text{Tr}(X_{I_1} \dots X_{I_k}). \quad (4.7)$$

The disorder averaging reduces to Wick contractions among the index sets  $I_k$ , as shown in eq(4.8). Each choice of contraction can be represented by a *chord diagram* with  $k$  nodes — corresponding to the insertions of  $X_I$  — arranged on a circle, reflecting the cyclicity of the trace (see [55] for more details). Chords connect pairs of nodes to indicate index contractions. This gives an infinite sum

$$\langle\langle\text{Tr}H^k\rangle\rangle = i^{\frac{kp}{2}} \binom{N}{p}^{-k/2} \sum_{\text{contractions}} \sum_{I_1, \dots, I_{\frac{k}{2}}} \text{Tr}(X_{I_1} X_{I_2} X_{I_1} \dots X_{I_k}). \quad (4.8)$$

If the chord diagrams are non-crossing — i.e., there are no intersections between chords — then the contracted fermion products are adjacent and square to the identity  $X_I^2 \propto \mathbb{I}$ . In the presence of chord crossings, the contracted fermion pairs can still be brought adjacent by commuting them, at the cost of introducing sign factors, since

$$X_I X_J = (-1)^{|I| \cap |J|} X_J X_I,$$

where  $|I| \cap |J|$  denotes the number of indices shared between the index sets  $I$  and  $J$ . In the double-scaled limit,  $|I| \cap |J|$  can be shown to be Poisson distributed, and this leads to the following result

$$\langle\langle\text{Tr}H^k\rangle\rangle = \sum_{\text{chord diagrams with } k \text{ nodes}} q^{\text{number of intersections}}. \quad (4.9)$$

A transfer matrix can be constructed for implementing this procedure, which acts on the Hilbert space of open chord states. Denoting the state with  $l$  open chords as  $|l\rangle$ , the moments of the Hamiltonian can be expressed as a simple transition amplitude

$$\langle\langle\text{Tr}H^k\rangle\rangle = \langle 0 | T^k | 0 \rangle,$$

where  $T$  is a transfer matrix operator explicitly defined in [39]. As a result, the partition function is given by

$$Z(\beta) = \langle 0 | e^{-\beta T} | 0 \rangle.$$

The spectrum of the transfer matrix  $T$  can be determined and is found to have finite width.

The final result, as derived in [39] by performing the infinite sum is,

$$Z(\beta) = \int_{-E_0}^{E_0} dE \rho(E) e^{-\beta E} = \int_0^\pi d\theta \Psi(\theta) e^{-\beta E(\theta)}, \quad (4.10)$$

where the width as well as the explicit density of states are given by

$$E_0 = \frac{2}{\sqrt{1-q}} \quad \text{and} \quad \rho(E) = \frac{\sqrt{1-q} (q; q)_\infty}{4\pi \sin \theta} (e^{\pm 2i\theta}; q)_\infty.$$

The answers are written in terms of the  $q$ -Pochhammer symbol  $(a; q)_\infty \equiv \prod_{k=0}^{\infty} (1 - aq^k)$ . We have also used here a convenient notation  $(e^{\pm ib}; q)_k \equiv (e^{ib}; q)_k (e^{-ib}; q)_k$ . In the second equality above for  $Z(\beta)$ , we have used a different angular variable  $\theta$  to parameterize the energy spectrum. It is related to actual energy via  $E(\theta) = -E_0 \cos \theta$ , and the corresponding density of states is

$$\Psi(\theta) = \frac{(1-q)^2 (q; q)_\infty^3}{2\pi} \frac{1}{|\Gamma_q(\frac{2i\theta}{\lambda})|^2}. \quad (4.11)$$

Here we encounter the  $q$ -Gamma function  $\Gamma_q(x) \equiv (1-q)^{1-x} \frac{(q; q)_\infty}{(q^x; q)_\infty}$ . As the name suggests, this is a generalization of the familiar Gamma function which is recovered in the  $q \rightarrow 1$  limit, i.e., we have  $\lim_{q \rightarrow 1} \Gamma_q(x) = \Gamma(x)$ .

To gain more insight into the spectrum described by above formulae, we plot in figure(15) the density of states  $\rho(E)$  for three different values of  $q$ .

- For  $q = 0$ , the density of states  $\rho(E)$  follows a semicircular distribution supported on  $-2 \leq E \leq 2$ ; the case  $q = 0.05$  in figure(15) closely resembles this expected form. We remind the reader that  $q \rightarrow 0$  corresponds to the limit where every term in the Hamiltonian describes a huge number of fermions interacting together.
- In contrast, for  $q = 1$ ,  $\rho(E)$  takes a Gaussian form, and the case  $q = 0.95$  shown in figure(15) approximates this behavior well. We remind the reader that  $q \rightarrow 1$  corresponds to the limit where every term in the Hamiltonian describes very few fermions interacting together.
- Notably, for finite  $q$  say  $q = 0.5$ , the density of states retains a semicircular shape near the spectral edges—as illustrated in fig(16a), while closely approximating a Gaussian in the bulk, as seen in fig(16b).

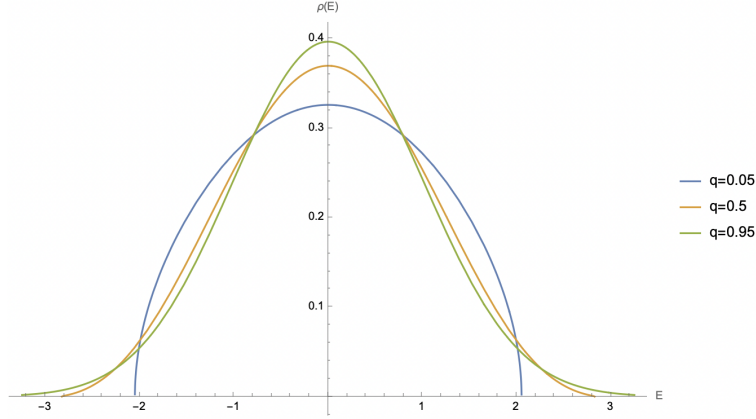


**Figure 15:** Density of states against energy for systems with different values of  $q$ .

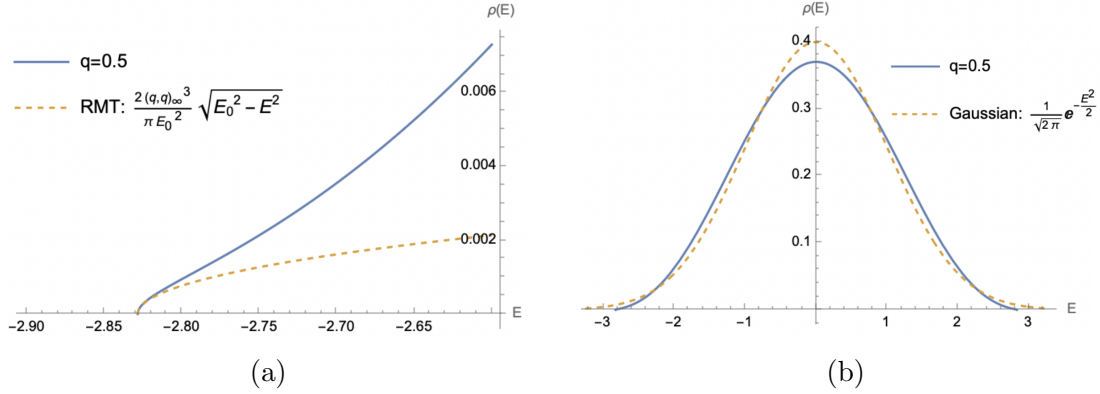


**Figure 16:** Density of states for finite  $q$  against semicircular and Gaussian density of states

Already in these asymptotic behaviors, we see the emergence of our toy models.

While the integral form of the partition function eq (4.10) is useful for understanding the dominant contributions at small  $\lambda$ , it is often convenient to work with a different representation for explicit calculations. In particular, the partition function admits a useful  $q$ -series expansion (see [40])

$$Z(\beta) = \frac{2}{\beta E_0} \sum_{p=0}^{\infty} (-1)^p q^{p+\binom{p}{2}} (2p+1) I_{2p+1}(\beta E_0), \quad (4.12)$$

where  $I_{2p+1}$  denotes the modified Bessel function. It will also be convenient to define

the object

$$Z_k(\beta) \equiv \langle k | e^{-\beta T} | 0 \rangle = \int_0^\pi d\theta \Psi(\theta) e^{\frac{2\beta \cos \theta}{\sqrt{1-q}}} \frac{H_k(\cos \theta | q)}{\sqrt{(q; q)_k}}, \quad (4.13)$$

where  $H_k(\cos \theta | q)$  are continuous  $q$  Hermite polynomials [56]. We mention some properties of  $Z_k$  in detail in Appendix(B).

**Two point function  $G(t)$  :** The chord diagram prescription introduced earlier in the context of partition functions extends naturally to the two point function of  $O$  operators we defined before. In the transfer matrix language, it leads to the same expression as in eq(2.4) (see [39]), with the averaged matrix elements being given by

$$\begin{aligned} f(E_1, E_2) &= \sum_k \tilde{q}^k \frac{H_k(-\frac{E_1}{E_0} | q) H_k(-\frac{E_2}{E_0} | q)}{(q; q)_k} \\ &= \frac{(1-q)^{-2m-3}}{(q; q)_\infty^3 \Gamma_q(2m)} (e^{\pm i\theta_1 \pm i\theta_2}; q)_m |\Gamma_q(\frac{i(\theta_1 + \theta_2)}{\lambda}) \Gamma_q(\frac{i(\theta_1 - \theta_2)}{\lambda})|^2, \end{aligned} \quad (4.14)$$

where again  $E_i = -\frac{2\cos \theta_i}{\sqrt{1-q}}$  in the second line above. One can check that to  $\mathcal{O}(\tilde{q})$ , the  $f(E_1, E_2)$  has the same form as the one assumed in RMT model eq(3.2). As with the partition function, a  $q$ -series expression can be derived for  $G(t)$ ,

$$G(t) = \frac{1}{Z(\beta)} \sum_{k=0}^{\infty} \tilde{q}^k Z_k(it) Z_k(\beta - it). \quad (4.15)$$

Since  $Z_k(\beta)$  has a  $q$  series expansion eq(B.1), this is a very explicit result. Below, we summarize additional useful properties of the DSSYK two-point function, beyond those discussed in section 2.1.

- **Identity operator case:** For  $\tilde{q} = 1$ , using the orthonormality property described in Appendix(B), we obtain  $G(t) = 1$ . This corresponds to the trivial case of the identity operator.
- **Short-time behavior of  $G(t)$ :** The two-point function has the following small time expansion:

$$G(t) = 1 - \frac{it(1-\tilde{q}) \partial_\beta Z(\beta)}{Z(\beta)} + \mathcal{O}(t^2). \quad (4.16)$$

This follows from the properties of  $Z_k$  in Appendix(B). The result is also consistent with the normalization  $G(t=0)$  being  $\beta$ -independent, as was assumed in section 2.

The key result of this section is the two point function of the DSSYK model given in eq(4.15). We conclude this subsection by highlighting a few special parameter choices where the DSSYK model reduces to simpler, analytically tractable models.

#### 4.1.1 Special Cases

The DSSYK model depends on the parameters:  $q$  and  $\tilde{q}$ . For certain special choices of these parameters, the model simplifies significantly, reducing to much simpler models, as outlined below.

- **RMT Model:** For  $q = \tilde{q} = 0$ , the DSSYK model reduces to the Random Matrix Theory (RMT) model. To see this, note that in this limit, the density of states and matrix elements simplify (eqn(4.11) and eqn(4.14)) to

$$\rho(E) = \frac{\sqrt{4 - E^2}}{2\pi}, \quad f(E_1, E_2) = 1, \quad (4.17)$$

matching the RMT case discussed in section 3.1 with the identification  $E_0 = 2$ ,  $\Delta = 0$ , and  $f_0 = 1$ . Consequently, all results for heat transport in this limit coincide with those of the RMT model.<sup>16</sup>

- **Gaussian Model:** In the case of  $q = 1$  and finite  $\tilde{q}$ , the model reduces to Gaussian model. This reduction is not immediately evident from the original DSSYK model expressions but becomes clear in the chord diagram formulation.

Recall the definition of the Hamiltonian moments in eq(4.9). When  $q = 1$ , the moments  $\text{Tr}\langle\langle H^{2k} \rangle\rangle$  simply count the number of Wick contractions among  $2k$  nodes, for which the generating function is a Gaussian. More explicitly, we have

$$\langle\langle \text{Tr} H^{2k} \rangle\rangle|_{q=1} = (2k - 1)!! = \int_{-\infty}^{\infty} dE \frac{e^{-\frac{E^2}{2}}}{\sqrt{2\pi}} E^{2k},$$

This then gives the density of states to be

$$\rho(E) = \frac{1}{J\sqrt{2\pi}} e^{-\frac{E^2}{2J^2}}, \quad (4.18)$$

which is the same as the result in section 3.3. Note that we have reinstated the disorder coupling  $J$  - previously set to 1 in eq(4.2). To compute the averaged matrix elements of operator  $f(E_1, E_2)$ , note that [57]

$$\lim_{q \rightarrow 1, \text{ fixed } E} \frac{H_k(-\frac{E}{E_0}|q)}{\sqrt{(q; q)_k}} = \frac{H_k(-\frac{E}{J\sqrt{2}})}{\sqrt{2^n n!}}, \quad E_0 = \frac{2J}{\sqrt{1-q}}, \quad (4.19)$$

---

<sup>16</sup>More generally, for small  $\tilde{q}$ , the DSSYK model continues to agree with the RMT model at leading order in  $\tilde{q}$ . At  $\mathcal{O}(\tilde{q})$ , this correspondence holds provided we identify the operator parameters as  $\Delta = \frac{4\tilde{q}}{1-q}$ ,  $f_0 = 1$ .

where  $H_k(x)$  is the Hermite polynomial. We can then obtain the function  $f(E_1, E_2)$  given in eq(4.14) to be<sup>17</sup>

$$f(E_1, E_2) = \frac{1}{\sqrt{1 - \tilde{q}^2}} e^{\frac{\tilde{q}}{2(1 - \tilde{q}^2)J^2} (2E_1 E_2 - \tilde{q}(E_1^2 + E_2^2))}. \quad (4.20)$$

This is identical to the expression in eq(3.20) with  $\gamma = 1, f_0 = 1$ . Consequently, all results for heat transport in this limit coincide with those of the gaussian model.

## 4.2 Regimes in the DSSYK model

The two-point function of the DSSYK model, given in eq(4.15) and eq(C.5), involves several parameters that make a general analysis nontrivial. However, by focusing on particular limits or parameter regimes, the model simplifies and as we will see reduces to well-understood physical systems. In this section, we explore such regimes, highlighting how they offer valuable physical intuition and how simple models can capture complicated dynamics of the DSSYK model.

Since this subsection involves a detailed exploration of a number of limits, we begin with a brief summary of the key regimes that arise in the DSSYK model.

- As we will show in section 4.2.2, the low-temperature, long-time limit ( $\beta \gg 1$ ) of DSSYK at finite  $q$  coincides with the behavior of the Cold RMT models introduced in section 3.1.1. We therefore refer to this as the *Cold RMT regime*. In this regime, the dynamics of DSSYK model is mostly governed by states near the ground state, where both the density of states and the matrix elements exhibit the same scaling as in random matrix theory. For instance, we will find that,  $\rho(E) \propto \sqrt{E - E_0}$  which is the same as the RMT (or cold RMT) spectrum near the edges.
- As  $q \rightarrow 1$ , or equivalently  $\lambda \rightarrow 0$ , the Cold RMT regime continues to exist in the low-temperature limit  $\beta \gg \lambda^{-\frac{3}{2}}$ . However, a distinct new regime emerges at higher temperatures,  $\beta \ll \lambda^{-\frac{3}{2}}$ , which we term the *Conformal regime*, detailed in section 4.2.1. More precisely the conformal regime is  $\lambda \rightarrow 0$  limit of the DSSYK model, with  $\beta\sqrt{\lambda}$  held fixed. In this regime, the density of states is approximately Gaussian in the angular variable  $\theta$ , and thermodynamics is dominated by states

---

<sup>17</sup>We have used the Mehler's formulae to perform the sum

$$\sum_{k=0}^{\infty} \frac{\tilde{q}^k H_k(-\frac{E_1}{\sqrt{2}}) H_k(-\frac{E_2}{\sqrt{2}})}{2^k k!} = \frac{1}{\sqrt{1 - \tilde{q}^2}} e^{\frac{\tilde{q}}{4(1 - \tilde{q}^2)} ((1 - \tilde{q})(E_1 + E_2)^2 - (1 + \tilde{q})(E_1 - E_2)^2)}.$$

near a saddle-point value of  $\theta$  determined by the combination  $\beta\sqrt{\lambda}$ . A schematic overview of these regimes is shown in figure(2).

We now turn to a detailed discussion of how these distinct regimes emerge from the DSSYK model. The results of this subsection is summarized in figure(1).

#### 4.2.1 Conformal Regime

The  $\lambda \rightarrow 0$  limit is the most well-studied regime of the DSSYK model [39, 40, 58], as this is where the low-energy dynamics of the SYK model are recovered. More precisely, the Schwarzian theory governing the infrared behavior of SYK emerges in the so-called *triple-scaling limit*[38], where  $\lambda \rightarrow 0$  with  $\beta\lambda^{\frac{3}{2}}$  held fixed. In this limit, both the partition function and the two-point function of the DSSYK model (with appropriately chosen  $m$ ) match those of the low-energy SYK model. In fact at all energies, the  $\lambda \rightarrow 0$  regime is equivalent to the large- $p$  limit of SYK with  $m = \frac{1}{p} \rightarrow 0$  as shown in [59]. We will now consider a somewhat different limit, which can be loosely seen as the high temperature version of the above limit where we take  $\lambda \rightarrow 0$ , with  $\beta\sqrt{\lambda}$  held fixed instead. In such a limit, we will soon see that the DSSYK model reduces to the conformal model that we discussed in section 3.2.

To see this, we first note that the density of states takes a simplified form in this limit (details in appendix(C)),

$$\frac{\Psi(\theta)}{E_0 \sin \theta} = \begin{cases} \frac{2\sqrt{2\pi}}{\lambda} e^{-\frac{\pi^2}{2\lambda} \theta} & \text{for } \theta \ll \lambda \\ \sqrt{\frac{2}{\pi}} e^{-\frac{2}{\lambda}(\frac{\pi}{2}-\theta)^2} & \text{for } \theta \gg \lambda \end{cases} \quad (4.21)$$

In the low-energy limit  $\theta \ll \lambda$ , the energy relation  $E + E_0 \approx \frac{\theta^2}{\sqrt{\lambda}}$  implies  $\rho(E) \propto \sqrt{E + E_0}$ , which matches the Cold RMT result given in eq(3.7) with  $\alpha = \frac{1}{2}$ . At low temperatures  $\beta \gg \lambda^{-\frac{3}{2}}$ , it turns out that only such low-energy states contribute, and the model effectively reduces to the Cold RMT regime described in section 3.1.1 - see Appendix(C) for more details. However, new physics arises in the opposite limit  $\beta \ll \lambda^{-\frac{3}{2}}$ , where contributions from states with  $\theta \gg \lambda$  dominate and will be the main focus of this section. We do the detailed analysis in Appendix(C), and here we give only the results.

The main simplification that occurs in the  $\beta \ll \lambda^{-\frac{3}{2}}$  regime is that the partition function turns out to have a saddle at some  $\theta$ . We will find it more useful to state the results in terms of the variable  $\phi \equiv \frac{\pi}{2} - \theta$ . Due to the saddle point, the thermodynamics is entirely dominated by states near  $\phi = \phi_0$  [39] where

$$\frac{4\phi_0}{\beta E_0 \lambda} = \cos \phi_0. \quad (4.22)$$

Note that  $\phi_0 \in (0, \frac{\pi}{2})$ . It is now simple to state the result for the two point function in terms of  $\phi_0$  which is [58]

$$\tilde{G}(\omega) = \frac{2(2 \cos \phi_0)^{2m-1}}{E_0 \lambda \Gamma(2m)} e^{\frac{\beta \omega}{2}} \Gamma(m + \frac{i\omega}{\lambda E_0 \cos \phi_0}) \Gamma(m - \frac{i\omega}{\lambda E_0 \cos \phi_0}). \quad (4.23)$$

We show in Appendix(C), the above result agrees qualitatively well with the numerical results even when  $\beta \sim \lambda^{-\frac{3}{2}}$ . The two-point function given in eq(4.23), exactly matches the conformal model result eq(3.15), upon choosing  $f_0 = 1$  and hence we term this regime as conformal regime.

It is sometimes useful to split the conformal regime into high and low temperature conformal regimes where it is possible to obtain analytic expressions for  $\phi_0$ . We have

$$\phi_0 = \begin{cases} \frac{\pi}{2}(1 - \frac{4}{\beta E_0 \lambda}) & \beta E_0 \lambda \gg 1, \text{ low temperature conformal regime} \\ \frac{\beta E_0 \lambda}{4} & \beta E_0 \lambda \ll 1, \text{ high temperature conformal regime} \end{cases} \quad (4.24)$$

**Spectral Function** As an aside, we compute the spectral function  $A(\omega)$  of the DSSYK model in the conformal regime via

$$A(\omega) = (1 + e^{-\beta \omega}) \tilde{G}(\omega).$$

We get

$$A(\omega) = \frac{\pi \cosh(\frac{\beta \omega}{2}) f_0 \beta (2 \cos(\phi_0))^{2m}}{2 \phi_0 \Gamma(2m) \sin(\pi m) \cosh(\frac{\pi \beta \omega}{4 \phi_0})} \text{Re} \left[ \frac{\Gamma\left(m - \frac{i\beta \omega}{4 \phi_0}\right)}{\Gamma\left(1 - m - \frac{i\beta \omega}{4 \phi_0}\right)} \right].$$

In the low temperature conformal limit,  $\phi_0 \rightarrow \frac{\pi}{2} - \frac{2\pi}{\beta E_0 \lambda}$  the above result with  $m = \frac{1}{4}$  matches exactly with the spectral function given for the SYK with four fermion interaction given in eq(8) of [35]<sup>18</sup>. Note that for more general  $m$ , the the temperature dependence is  $A(\omega) \sim \beta^{1-2m}$ .

#### 4.2.2 Cold RMT regime

At long times, we can obtain an explicit expression for the two-point function for the DSSYK model using the  $q$ -series expression given in eq(4.15). Since  $Z_k$  itself is a  $q$ -series (see eq(B.1)) involving Bessel functions, we employ the asymptotic expansion of the Bessel function at large arguments (see Appendix B.1 for details) to extract the

---

<sup>18</sup>In the DSSYK model, the parameter  $m = \frac{\tilde{p}}{p}$  is the number of fermions in the operator divided by the number of fermions in the Hamiltonian. For the SYK<sub>4</sub> Hamiltonian of reference [35],  $p = 4$  since the Hamiltonian is quartic in fermions and  $\tilde{p} = 1$ , since they compute the two point function of a single fermion. Hence  $m = \frac{1}{4}$ . We also have to take their  $J^2 = \frac{\lambda}{4\pi}$ .

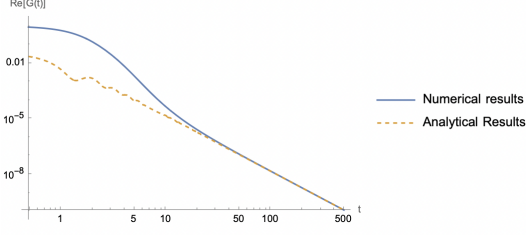


**Figure 17:**  $\text{Re}[G(t)]$  vs  $t$  for  $q = \tilde{q} = 0.5$ ,  $\beta = 1$

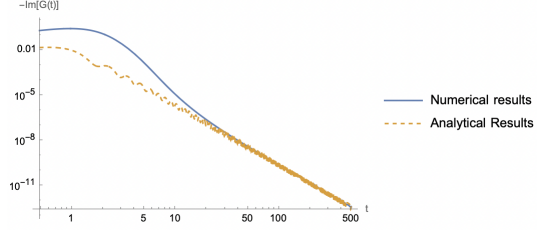


**Figure 18:**  $\text{Im}[G(t)]$  vs  $t$  for  $q = \tilde{q} = 0.5$ ,  $\beta = 1$

large-time behavior. The resulting expression for the two-point function is valid for finite  $q$  in the regime  $t \gg 1$ ,

$$G(t) = \frac{4(q; q)_\infty^6 (\tilde{q}^2; q)_\infty}{\pi E_0^3 (t(t + i\beta))^{\frac{3}{2}} Z(\beta)} \left( \frac{\cosh(E_0 \beta)}{(\tilde{q}; q)_\infty^4} - \frac{\sin(2E_0 t + iE_0 \beta)}{(-\tilde{q}; q)_\infty^4} \right). \quad (4.25)$$

It is interesting to note that the time dependence of  $G(t)$  matches that of the RMT models, as given in eq(3.5). Before discussing the physical implications, we verify numerically the validity of the above result. This is illustrated in figures 17 and 18, where we plot  $\text{Re} G(t)$  and  $\text{Im} G(t)$  as functions of  $t$  for a specific set of parameters, and observe good agreement with eq(4.25) at large times. One can also extract a characteristic timescale, the *scrambling time*  $t_s$ , which we define here as the time beyond which the two-point function is well approximated (within 10% accuracy) by the expression in eq(4.25).<sup>19</sup> To characterize the scale  $t_s$  as a function of  $\lambda$ , we plot  $t_s$  v/s  $\lambda$  for a few different values of  $\beta$  (fig(19)). It is observed that  $t_s$  is well approximated by the relation  $t_s \sim \frac{20}{3} \frac{1}{\lambda^{\frac{3}{2}}}$  over a wide range of  $\beta$ , namely  $0.01 \leq \beta \leq 10$ . In what follows, we show that the low temperature long time limit of DSSYK ( $\beta, t \gg 1$ ) matches exactly to cold RMT model by comparing the DSSYK partition function and the two point function. The matching of partition function is as follows : In the low-temperature limit, the DSSYK model is sensitive only to states near the ground state at  $E = -E_0$ . From eq(4.11), we obtain

$$\lim_{E \rightarrow -E_0} \rho(E) = \frac{2(q; q)_\infty^3}{\pi E_0^2} \sqrt{E_0^2 - E^2},$$

which matches the density of states of the cold RMT model given in eq(3.7) with  $\alpha = \frac{1}{2}$ , upon appropriate choice of the normalization constant  $\mathcal{N}_r$ . Furthermore, the two-point function given in eq(4.25), together with the already-matched partition function

<sup>19</sup>Actually we use just the  $\text{Re}(G(t))$  to extract  $t_s$ , since the  $t_s$  extracted from the  $\text{Im}(G(t))$  is fairly close

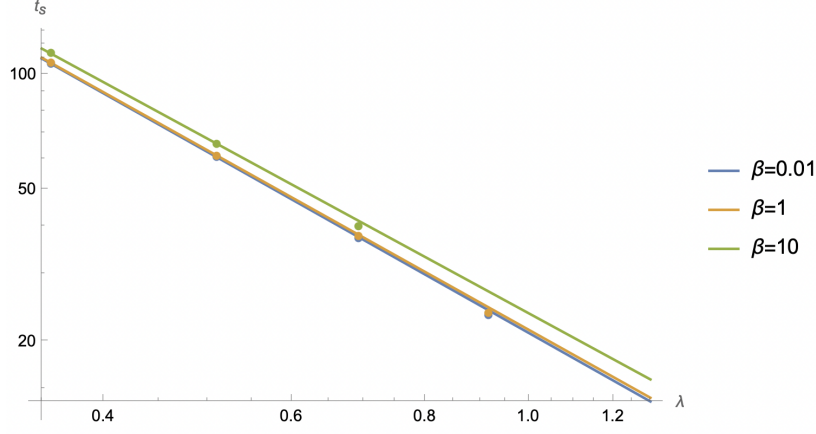


**Figure 19:**  $\lambda$  vs  $t_s$  for three  $\beta$  values;  $t_s \sim \frac{20}{\lambda^{\frac{3}{2}}}$

$Z(\beta)$ , agrees exactly with the two-point function of the RMT model<sup>20</sup> given in eq(3.5), provided the RMT parameters  $f_0$  and  $\Delta$  are appropriately identified.

In summary, the DSSYK model with parameters  $(q, \tilde{q})$  in the cold RMT regime, namely  $\beta, t \gg 1$ , matches the cold RMT model described in section 3.1.1, characterized by the parameters  $f_0, \mathcal{N}_r, \Delta$ , and  $\alpha = \frac{1}{2}$ , under the following identification<sup>21</sup>

$$\begin{aligned}
 \mathcal{N}_r &= (q, q)_\infty^3, \\
 f_0 &= \frac{1}{2}(\tilde{q}^2; q)_\infty \left[ (-\tilde{q}, q)_\infty^{-4} + (\tilde{q}, q)_\infty^{-4} \right], \\
 \frac{1 + \Delta}{1 - \Delta} &= \frac{(-\tilde{q}; q)_\infty^4}{(\tilde{q}; q)_\infty^4}.
 \end{aligned} \tag{4.26}$$

One can also explicitly verify that  $1 > \Delta > -1, f_0 > 0$ , as anticipated in section 3.1. The discussion above was for finite  $q$ . As is clear from the discussion below eq(4.21), for  $q \rightarrow 1$  or  $\lambda \rightarrow 0$ , the cold RMT regime emerges in the limit  $t, \beta \gg \lambda^{-\frac{3}{2}}$  with the same matching of parameters as in eq(4.26).

### 4.3 Transport in DSSYK Models

In this section we examine the heat transport in the DSSYK model. As discussed in the introduction the typical heat current plot given in fig(3) has an initial increase to

<sup>20</sup>We have already mentioned in section 3.1.1 that at low temperatures and long times, the two-point functions of the cold RMT and the RMT models coincide.

<sup>21</sup>This result can also be obtained by matching the matrix elements. The function  $f(E_1, E_2)$  in DSSYK, given in eq(4.14), can be expanded near the left edge of the spectrum ( $E \approx -E_0$ ) to quadratic order and compared with the RMT result in eq(3.2).

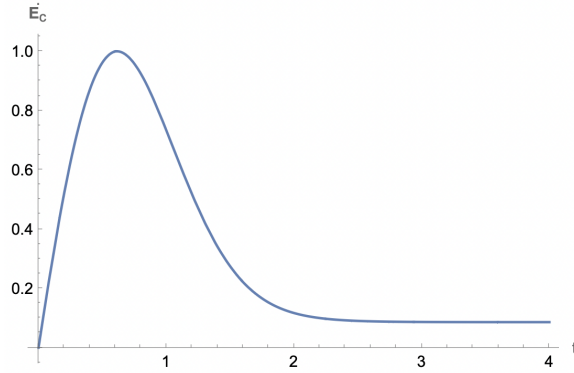


**Figure 20:** Heat Current vs time for a DSSYK system with  $q = 0.5, \beta = 1$

a peak value and eventually settles down to constant value. The DSSYK model heat current exhibits these features as expected - the plot of heat current for some typical values of DSSYK parameters are given in fig(20) which clearly shows the initial increase and eventual NESS regime. For the case of DSSYK, the initial increase can be worked out analytically and it turns out to be linear in time. Using the small  $t$  expansion of two point function given in eq(4.16), the heat current at small time is obtained to be

$$\dot{E}_c(t) = \frac{2(1 - \tilde{q})\epsilon^2 \partial_\beta Z(\beta)}{Z(\beta)} t + \mathcal{O}(t^2). \quad (4.27)$$

Notice that the RHS above is proportional to the internal energy of the DSSYK system. This means that, for small times, the fractional change in energy of the DSSYK system is independent of  $\beta$ . The eventual saturation in heat current happens since for sufficiently long time, the DSSYK model reduces to an RMT model as discussed in section 4.2.2.

As we saw in the previous section, in specific (not necessarily distinct) limits the DSSYK model reduces to the simple models introduced in sections 3.1-3.3 as summarized in figure(1). We expect that the heat current for the DSSYK model in those specific limits will be captured well by the appropriate toy models. We first present the analytical results obtained for the  $\lambda \rightarrow 0$  case for conductivities at different temperature limits. In section 4.3.2, we give the typical plots of heat currents against RMT and Conformal model results and provide numerical evidence showing that the behavior away from the *RMT* and *Conformal* regimes smoothly interpolates between these analytical regimes.

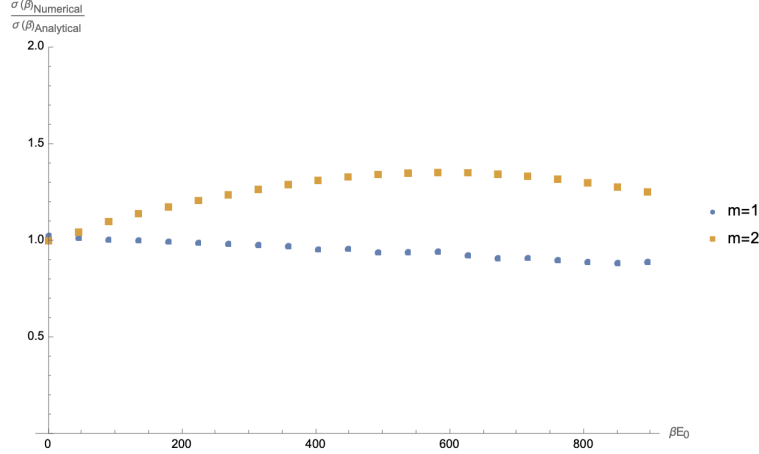


**Figure 21:** Ratio of numerical values of  $\sigma(\beta)$  against analytical result for  $\lambda = 0.05$  and different values of  $m$ .

#### 4.3.1 DSSYK Model in the conformal regime $\lambda \rightarrow 0$

In the conformal regime, i.e  $\lambda \rightarrow 0, \beta \ll \lambda^{-\frac{3}{2}}$ , as discussed in section 4.2.1, the two point function agrees with the conformal toy model 3.2. Hence the conductivity in this regime can be read off from the results of the conformal model given in eq(3.17) with appropriate  $\phi_0$ . More explicitly, we have the conductivity of the DSSYK model in the conformal regime

$$\sigma = c_m \epsilon^2 f_0^2 \phi_0 \beta \cos^{4m}(\phi_0), \quad \frac{4\phi_0}{\beta E_0 \lambda} = \cos \phi_0, \quad (4.28)$$

where  $c_m \equiv 2\sqrt{\pi} m^2 \frac{\Gamma(2m)}{\Gamma(2m+\frac{3}{2})}$ . We check numerically in figure(21) that the conductivity for the DSSYK model agrees with the above formulae very well. Note that even outside the conformal regime, say around  $\beta E_0 \sim \frac{1}{\lambda^2}$  as we see in figure(21) the conformal regime results are only a few percentages off from the actual result at least for  $m = 1$  case. We end with some explicit results for the conductivity  $\sigma$  of the DSSYK model in the low and high temperature conformal regime,

- **Low temperature conformal regime**  $\frac{1}{\lambda} \gg \beta \sqrt{\lambda} \gg 1$  :

$$\sigma \approx \frac{1}{2} \epsilon^2 f_0^2 c_m \pi^{1+4m} \lambda^{-2m} \beta^{1-4m} \quad (4.29)$$

- **High temperature conformal regime**  $1 \gg \beta \sqrt{\lambda}$

$$\sigma \approx \frac{\epsilon^2}{2} f_0^2 c_m \sqrt{\lambda} \beta^2 \quad (4.30)$$

**Comparison to results in literature** In this subsection we obtained results about heat transport between two DSSYK systems in the conformal regime. As mentioned before, the low temperature conformal regime of DSSYK model with  $m = \frac{1}{p}$  matches the low temperature SYK<sub>*p*</sub> models. Hence the results for transport in the DSSYK model in this regime must match with that of the low temperature SYK <sub>$\frac{1}{m}$</sub>  model.

In the work [35], the authors couple two SYK<sub>4</sub> systems via a free fermion channel (or equivalently a SYK<sub>2</sub> system). While this setup is not exactly the same as ours, we can easily construct a setup similar to theirs by connecting two of our setups. Then their conductivity can be extracted just from the conductivity between the SYK<sub>4</sub> system and the channel SYK<sub>2</sub> system. In eq(3.18), we already have worked out the conductivity between two different conformal systems - upon using  $m_c = \frac{1}{4}, m_h = \frac{1}{2}$  the conductivity is obtained to be

$$\sigma \sim \beta^{-\frac{1}{2}} = \sqrt{T}, \quad (4.31)$$

which agrees with the weak coupling results of [35]. Additionally, when the coupling between the SYK<sub>4</sub> and SYK<sub>2</sub> systems is very strong, the authors of [35] find that the conductivity behaves as  $\sigma \sim T$ . It is interesting to note that this result is also reproduced by the weak coupling calculation discussed above, provided we replace  $m_c = \frac{1}{4} \rightarrow \frac{1}{2}$ . We leave a detailed exploration of this apparent connection (if any) to future work.

#### 4.3.2 Numerical results for heat transport in DSSYK for $t < (1 - q)^{-\frac{3}{2}}$ and finite $\lambda$

In this section, we focus on the large-time behavior of systems with finite  $q$  values, specifically analyzing the quantity  $\dot{E}_-(t)$ , which was defined in eq(2.9). As discussed in the introduction, at late times,  $\dot{E}_-(t)$  becomes the dominant contribution to the heat current, making it the relevant observable in this regime. The intermediate  $q$  does not quite reduce to any of our toy models. However, what we see numerically is that there is still an interpolation *in time* between the conformal and RMT regimes. This suggests that, in some sense, the intermediate  $q$  DSSYK can be thought of as RG running from the conformal model at high temperatures/small times to a RMT-like model at low temperatures/large times.

To explore this, we compare numerical results for  $\dot{E}_-(t)$  with that of the RMT and conformal toy models at two different inverse temperatures,  $\beta = 1$  and  $\beta = 100$  in figure(22).

- For  $\beta = 1$ , it is seen that the system reaches non equilibrium steady state (NESS) fairly quickly around  $t > 1$  and the NESS regime heat current turns out to match that of the conformal toy model as shown in the figure(22a). In computing the

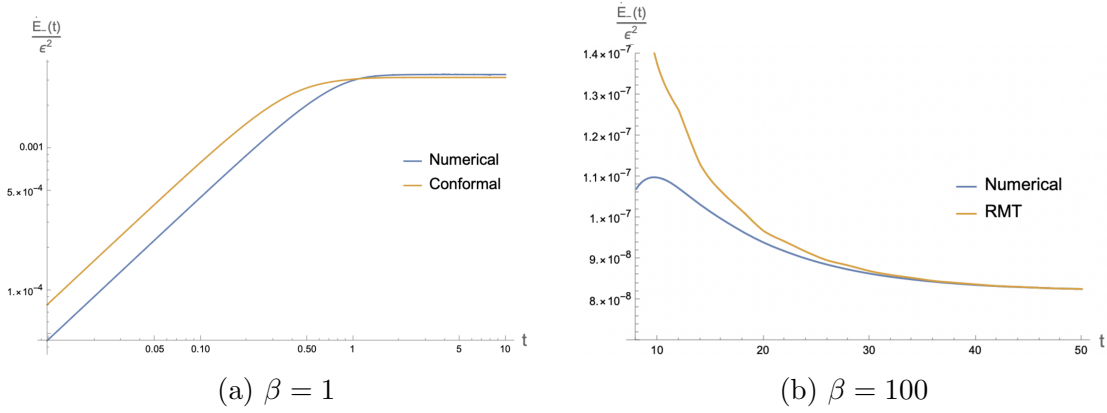


**Figure 22:**  $\dot{E}_-(t)$  results for  $q = 0.4$  and different values of  $\beta$  against corresponding results for conformal model and RMT results. We have normalized the RMT results so that it agrees with the DSSYK results at  $t = 50$ .

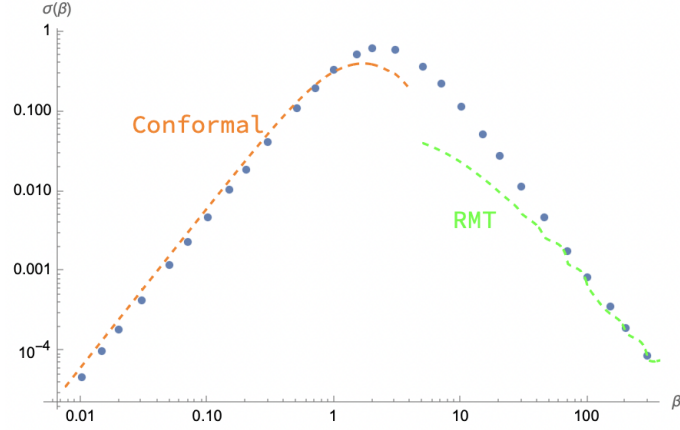
heat current for the conformal case in the figure(22a), we use the conformal two point function given in eq(3.14) with  $\phi_0$  found by solving eq(4.22).

- At lower temperatures say  $\beta = 100$ , around time  $t \gtrsim 50$ , does not exactly match RMT. But, we see that, with an appropriate normalization, RMT does get the fall off right - see figure(22b). In computing the heat current for the RMT case in the figure(22b), we use the two point function given in eq(3.5) with parameters as given in eq(4.26).

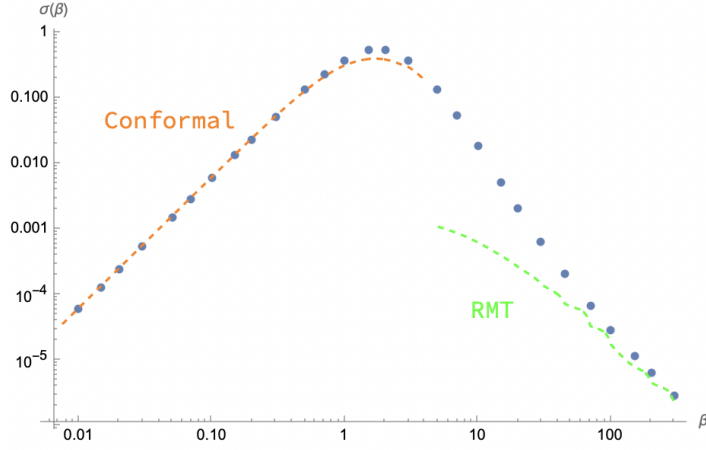
We thus observe numerically that the crossover between RMT-like and conformal like behavior figure(2), previously observed in the  $q \rightarrow 1$  regime, persists even at finite  $q$  values.

**Finite  $q$  conductivity:** In the above discussion, we observed that the NESS heat current of the DSSYK model matches the results of the conformal and RMT toy models in the high- and low-temperature limits, respectively. This behavior is also reflected in the thermal conductivity. In figure(23), we plot the thermal conductivity  $\sigma$  as a function of temperature for the DSSYK model, RMT toy model, and conformal toy model for a few different values of  $m$ . As expected, we find good agreement between the DSSYK model and the conformal model at high temperatures ( $\beta < \beta_d$  with  $\beta_d \sim 1$ ), and with the RMT toy model at low temperatures ( $\beta > \beta_s$  with  $\beta_s \sim 70$ ).

In fact, we can make this observation more quantitative by defining  $\beta_d^{-1}$  as the temperature above which the DSSYK conductivity deviates from the RMT result by more than 50%, and  $\beta_s^{-1}$  as the temperature below which the DSSYK conductivity



(a)  $m = 1$



(b)  $m = 2$

**Figure 23:** Numerical values of  $\sigma(\beta)$  vs Conformal model and Cold RMT results for  $q = 0.4$  and  $m = 1, m = 2$ .

deviates from the conformal result by more than 20%. In figure(24), we plot  $\beta_s$  and  $\beta_d$  as functions of  $\lambda$ . At finite  $\lambda$ , the transition between conformal vs RMT regimes is not as sharp in temperature as suggested by fig(2). Numerics suggests an intermediate region between the temperatures  $\beta_s^{-1}$  and  $\beta_d^{-1}$ , that separates a low temperature RMT-like behavior from a high temperature conformal-like behavior.

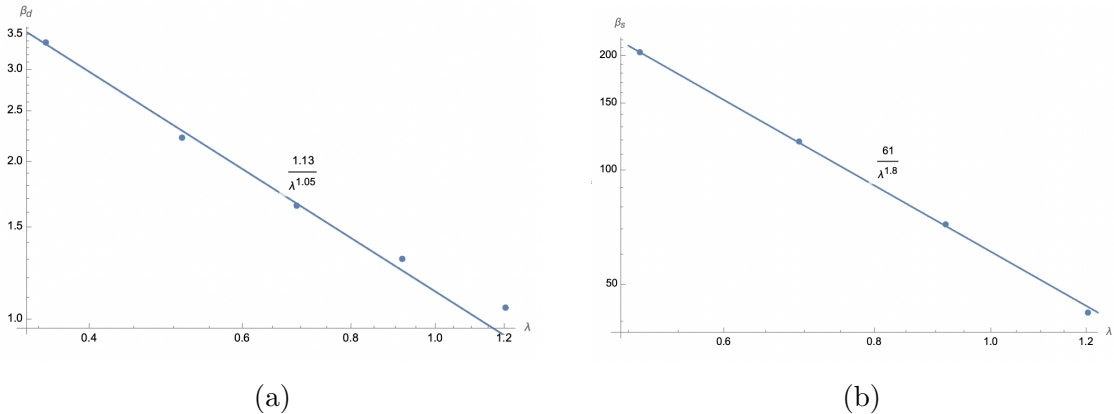


**Figure 24:**  $\beta_s$  and  $\beta_d$  plotted against corresponding values of  $\lambda$ .

## 5 Conclusions and Outlook

In this work, we have analyzed the heat transport between two quantum systems using a set of exactly solvable models. We demonstrated that even relatively simple toy models - motivated by random matrix theory and conformal symmetry - are sufficient to capture a number of essential features of thermal transport, including the approach to non-equilibrium steady state. We also worked out the transport in the case of solvable but nontrivial case of DSSYK models. We showed that the behavior of heat transport in the DSSYK systems interpolate smoothly between the conformal and the RMT toy model results models with the transition temperature  $\sim \lambda^{-\frac{3}{2}}$ . The behavior of the DSSYK model appears suggestive of an RG flow between conformal and RMT regimes.

We end with some comments on interesting future directions. An obvious question is to investigate higher order corrections in coupling strength  $\epsilon$  between the systems. At higher order, the heat current will depend on higher-point correlation functions. In the context of DSSYK model, this question is accessible - although more complicated than the two point function results and may reveal new regimes of behavior. It would be interesting to see if there is a new scaling regime as happens in the SYK case [35].

Another interesting direction is to investigate transport in other solvable versions of the DSSYK model [49–51] with more symmetries, where an even richer behavior is expected. Apart from introducing extra parameters, one could also study charge transport rather than just the heat transport. A different kind of extension is to consider a chain made of the kind of toy models we consider here, as well as a DSSYK chain.<sup>22</sup> This would allow us to see how our statements extend to higher dimensional

<sup>22</sup>See [60, 61] for related construction.

heat transport.

In this work, we have refrained from commenting on the possible holographic interpretation of our results. There are many existing proposals for the gravitational duals for DSSYK[46, 48]. It would be interesting to give a gravitational picture of various regimes we see in this work.

We conclude with the hope that the exact results obtained here will lead to deeper insights into quantum transport.

## Acknowledgments

We would like to acknowledge discussions with Subhro Bhattacharjee, Abhishek Dhar, Manas Kulkarni, Gautam Mandal, Shiraz Minwalla, Sandip Trivedi and Spenta Wadia. This work was presented at the GautamFest Conference at TIFR Mumbai in January 2025, and at the ICTS-TIFR string seminar in March 2025. RL thanks the organizers of both for giving him the opportunity to present this work. RL acknowledges the support of the Department of Atomic Energy, Government of India, under project no. RTI4001, and would also like to acknowledge his debt to the people of India for their steady and generous support of research in the basic sciences. PN would like to acknowledge SERB grant MTR/2021/000145.

## A Expression for energy current

We compute the expectation value of  $E_c$  corresponding to the coupled quantum system discussed in section 2. Alternately, we could have started with a finite temperature state of the two systems (same on both sides) and turn on the interaction Hamiltonian (at time  $t = 0$  say) and ask about the quenching of the system. More precisely we will be interested in the object,<sup>23</sup>

$$E_c(t) \equiv \frac{1}{Z} \text{Tr} [H_c(t) \rho_0], \quad \rho_0 \equiv e^{-\beta_c H_c} e^{-\beta_h H_h}, \quad Z(\beta) = \text{Tr} [\rho_0] . \quad (\text{A.1})$$

We compute the above quantity to  $\mathcal{O}(\epsilon^2)$ . To evaluate this, we can go to the interaction picture by defining  $\mathcal{H} = H_0 + H_I$  in the Hamiltonian eq(2.1) with  $H = H_c + H_h$  and  $H_I = \epsilon O_c O_h \theta(t)$ . Denoting the interaction picture operators and states by the superscript  $^{(0)}$ , for instance  $H_I^{(0)}(t) = e^{iH_0 t} H_I e^{-iH_0 t}$  or  $\rho_0^{(0)}(t) = U(t) \rho_0 U^\dagger(t)$  where  $U(t) \equiv e^{iH_0 t} e^{-iH t}$  is the interaction picture evolution operator. The energy expectation value is thus given by,

$$Z E_c(t) = \text{Tr} \left[ H_c^{(0)}(t) \rho_0^{(0)}(t) \right] = \text{Tr} \left[ U^\dagger(t) H_c U(t) \rho_0 \right] \quad (\text{A.2})$$

---

<sup>23</sup>For SYK the equation involves disorder averaging, hence  $E_c(t) \equiv \frac{1}{Z} \langle \text{Tr} [H_c(t) \rho_0] \rangle$

We now expand  $U(t)$  perturbatively in  $\epsilon$ . We thus have the following result where ,

$$\dot{E}_c(t) = \frac{1}{Z} (-i\epsilon)^2 \int_0^{t_1} dt_2 \text{Tr} \left[ [H_I^{(0)}(t_1), [H_I^{(0)}(t_2), H_c]] \rho_0 \right] \quad (\text{A.3})$$

Now we factorize the Hilbert space<sup>24</sup>,

$$\begin{aligned} \dot{E}_c(t) &= -\frac{\epsilon^2}{Z} \int_0^{t_1} dt_2 \left( \text{Tr} [O_c(t_1) [O_c(t_2), H_c] e^{-\beta_c H_c}] \text{Tr} [O_h(t_1) O_h(t_2) e^{-\beta_h H_h}] \right. \\ &\quad \left. - \text{Tr} [[O_c(t_2), H_c] O_c(t_1) e^{-\beta_c H_c}] \text{Tr} [O_h(t_2) O_h(t_1) e^{-\beta_h H_h}] \right) \\ &= -\epsilon^2 \int_0^{t_1} dt_2 \left( i (\partial_{t_2} G_c(t_1 - t_2)) G_h(t_1 - t_2) - i (\partial_{t_2} G_c(t_2 - t_1)) G_h(t_2 - t_1) \right) \\ &= -2\epsilon^2 \int_0^{t_1} d\tilde{t} \text{Im} (\partial_{\tilde{t}} G_c(\tilde{t}) G_h(\tilde{t})) \\ &= -\epsilon^2 \text{Im} \left( G_c(t_1) G_h(t_1) + \int_0^{t_1} d\tilde{t} [\partial_{\tilde{t}} G_c(\tilde{t}) G_h(\tilde{t}) - G_c(\tilde{t}) \partial_{\tilde{t}} G_h(\tilde{t})] \right) \end{aligned} \quad (\text{A.4})$$

In going to the third line, we have used  $G^*(-t) = G(t)$ . Since  $G(t=0) = 1$  is real, we have also dropped  $G_c(0)G_h(0)$  term in the last expression. We thus get eq(2.9).

## B Properties of $Z_k$

In this appendix, we elaborate on the properties of the quantities  $Z_k(\beta)$ , defined in eq(4.13), which play an important role in the analysis of the DSSYK model. We begin by listing the key properties of  $Z_k$ , followed by a detailed discussion of their asymptotic behavior, which ultimately leads to the result in eq(4.25). A particularly useful representation of  $Z_k(\beta)$  is given by the following  $q$ -series expansion, analogous to that of the partition function:

$$Z_k(\beta) = \frac{2}{\beta E_0} \sum_{p=0}^{\infty} \frac{(-1)^p q^{p^+ \binom{p}{2}} (k+2p+1)(q; q)_{k+p}}{(q; q)_p \sqrt{(q; q)_k}} I_{k+2p+1}(\beta E_0) \quad (\text{B.1})$$

---

<sup>24</sup> For the SYK systems considered in this paper, the intermediate steps are slightly different since we need to perform disorder averages, but the final result eq(A.4) is the same. To see this, note that the heat current in the SYK case can be written as,

$$\dot{E}_c(t) = -\epsilon^2 \frac{i^{p_{\bar{c}}+p_{\bar{h}}}}{Z_c Z_h} \int_0^{t_1} dt_2 \langle \langle \text{Tr} \left( [J_{\bar{I}, \bar{A}} X_{\bar{I}}^{(0)}(t_1) Y_{\bar{A}}^{(0)}(t_1), [J_{\bar{J}, \bar{B}} X_{\bar{J}}^{(0)}(t_2) Y_{\bar{B}}^{(0)}(t_2), H_c] \right) \rho_0 \rangle \rangle$$

where  $\langle \langle \dots \rangle \rangle$  denotes the disorder average. We can further use the factorization property of the disorder average,  $\langle \langle J_{\bar{I}, \bar{A}} J_{\bar{J}, \bar{B}} \rangle \rangle = \langle \langle J_{\bar{I}} J_{\bar{J}} \rangle \rangle \langle \langle J_{\bar{A}} J_{\bar{B}} \rangle \rangle$  to simplify the expression leading the second line of eq(A.4).

The quantity  $Z_k(\beta)$  has many useful structural properties which will be used throughout the main analysis ,

- **Orthonormality:**

$$\sum_{k=0}^{\infty} Z_k(\beta_1) Z_k(\beta_2) = Z(\beta_1 + \beta_2).$$

This follows by inserting (4.13) for both  $Z_k$ 's, using the completeness relation

$$\sum_{k=0}^{\infty} \frac{H_k(\cos \theta_1 | q) H_k(\cos \theta_2 | q)}{(q; q)_k} = \frac{\delta(\theta_1 - \theta_2)}{\Psi(\theta_1)},$$

which collapses one integration and yields  $Z(\beta_1 + \beta_2)$ .

- **Recursion relation:**

$$\sqrt{1-q} \partial_\beta Z_k(\beta) = \sqrt{1-q^{k+1}} Z_{k+1}(\beta) + \sqrt{1-q^k} Z_{k-1}(\beta).$$

This is obtained by differentiating (4.13) with respect to  $\beta$  and using the recurrence

$$2 \cos \theta H_k(\cos \theta) = \sqrt{1-q^{k+1}} H_{k+1} + \sqrt{1-q^k} H_{k-1},$$

then recognising the resulting integrals as  $Z_{k\pm 1}(\beta)$ .

- $\beta = 0$  **case:**

$$Z_k(0) = \delta_{k,0}.$$

Setting  $\beta = 0$  makes the exponential unity; orthogonality of  $H_k$  then gives  $\delta_{k,0}$ .

- $k = 0$  **case:**

$$Z_0(\beta) = Z(\beta).$$

This follows directly from  $H_0 = 1$  and  $(q; q)_0 = 1$  in (4.13).

## B.1 Long-Time Limit of the Two-Point Function $Z_k(\beta)$

In this subsection, we determine the large- $t$  behavior of  $Z_k(it)$  and  $Z_k(\beta - it)$ , since the two-point function is expressed in terms of these in eq(4.15). To study the large- $t$  limit, we note that  $Z_k(\beta)$  admits a  $q$ -series representation given in eq(B.1), which involves modified Bessel functions of the first kind. This structure allows us to use the known asymptotic forms of the Bessel functions to evaluate  $Z_k(\beta)$  in the appropriate limit. Consequently, we obtain the long-time behavior of the two-point function, as summarized in eq(4.25). The relevant asymptotics of the Bessel function  $I_\nu(z)$  for integer  $\nu$  is as follows (see Section 8.451 of [62]),

- For  $\tau$  away from the positive imaginary axis

$$I_\nu(\tau) \approx \frac{e^\tau - i(-1)^\nu e^{-\tau}}{\sqrt{2\pi\tau}}, \quad |\tau| \rightarrow \infty, -\frac{3\pi}{2} < \arg \tau < \frac{\pi}{2} \quad (\text{B.2})$$

- For  $\tau$  away from negative imaginary axis we have,

$$I_\nu(\tau) \approx \frac{e^\tau + i(-1)^\nu e^{-\tau}}{\sqrt{2\pi\tau}}, \quad |\tau| \rightarrow \infty, -\frac{\pi}{2} < \arg z < \frac{3\pi}{2} \quad (\text{B.3})$$

– As a special case of eq(B.3), we also have that

$$\lim_{t \rightarrow \infty} I_\nu(it) = \sqrt{\frac{2}{\pi t}} \begin{cases} \sin\left(\frac{\pi}{4} + t\right) & \text{if } \nu \in \text{even} \\ -i \cos\left(\frac{\pi}{4} + t\right) & \text{if } \nu \in \text{odd} \end{cases} \quad (\text{B.4})$$

$Z_k(\beta - it)$  **at large  $t$**  : We will first compute  $Z_k(\beta - it)$  at large  $t$ . Since this the argument is away from the positive imaginary axis, we can use eq(B.2). We then get

$$\lim_{|\beta - it| \rightarrow \infty} Z_k(\beta - it) = \frac{(1 - q)^{\frac{3}{4}}}{2\sqrt{\pi}} \frac{C_{q,k}}{(\beta - it)^{\frac{3}{2}}} \left( e^{\frac{2(\beta - it)}{\sqrt{1-q}}} + i(-1)^k e^{\frac{-2(\beta - it)}{\sqrt{1-q}}} \right) \quad (\text{B.5})$$

where  $C_{q,k} \equiv \sum_{p=0}^{\infty} \frac{(-1)^p q^{p+\binom{p}{2}} (k+2p+1)(q;q)_{k+p}}{(q;q)_p \sqrt{(q;q)_k}} = \frac{(q;q)_\infty^3 H_k(1|q)}{\sqrt{(q;q)_k}}$ <sup>25</sup>.

$Z_k(it)$  **at Long Time** : Now we compute the next ingredient in eq(4.15), namely  $Z_k(it)$  at large  $t$ . Plugging in the result eq(B.4), we get

$$\lim_{t \rightarrow \infty} Z_k(it) = -\frac{(1 - q)^{\frac{3}{4}} (q;q)_\infty^3 H_k(1|q)}{\sqrt{\pi t^3} \sqrt{(q;q)_k}} \begin{cases} i \sin\left(\frac{\pi}{4} + \frac{2t}{\sqrt{1-q}}\right) & \text{if } k \in \text{odd} \\ \cos\left(\frac{\pi}{4} + \frac{2t}{\sqrt{1-q}}\right) & \text{if } k \in \text{even} \end{cases} \quad (\text{B.7})$$

---

<sup>25</sup>The last equality can be checked numerically. We can also obtain the same result by evaluating the  $Z_k$  given as an integral in eq(4.13) in the long time regime. In this regime, the integral is expected to be dominated by contributions near the edges of the distribution,  $\theta = 0$  and  $\theta = \pi$ . It can thus be split into two parts, with each integrand expanded around its respective edge. After a change of variables near  $\theta = \pi$ , we obtain:

$$\begin{aligned} Z_k(\beta - it) &= \frac{2(q;q)_\infty^3}{\pi \sqrt{(q;q)_k}} H_k(1|q) \left( e^{\frac{2(\beta - it)}{\sqrt{1-q}}} \int_0^{\frac{\pi}{2}} d\theta \theta^2 e^{-\frac{(\beta - it)\theta^2}{\sqrt{1-q}}} + (-1)^k e^{\frac{-2(\beta - it)}{\sqrt{1-q}}} \int_0^{\frac{\pi}{2}} d\theta \theta^2 e^{\frac{(\beta - it)\theta^2}{\sqrt{1-q}}} \right) \\ &= \frac{(q;q)_\infty^3 (1 - q)^{\frac{3}{4}} H_k(1|q)}{2\sqrt{(\pi)}(\beta - it)^{\frac{3}{2}}} \left( e^{\frac{2(\beta - it)}{\sqrt{1-q}}} + i(-1)^k e^{\frac{-2(\beta - it)}{\sqrt{1-q}}} \right) \end{aligned} \quad (\text{B.6})$$

where the upper limit is changed to  $\infty$  as the integral gets contribution only from  $\theta \approx 0$ . Comparing this result against B.5,  $C_{q,k}$  can be read off to be  $\frac{(q;q)_\infty^3 H_k(1|q)}{\sqrt{(q;q)_k}}$

With both ingredients in eq(4.15) now determined, we can proceed to assemble them and obtain the two point function as given in eq(4.25).<sup>26</sup>

## C Additional details of DSSYK in conformal Regime

In this appendix, we elaborate on the details of the calculations in the conformal regime. We first discuss the simplifications that occur in the limit  $\lambda \rightarrow 0$ , where the model becomes analytically tractable. Following this, we present explicit expressions for the partition function and the two-point function in the high-temperature limit  $\beta \ll \lambda^{-\frac{3}{2}}$ .

**Density of states:** The key simplification of the density of states (eqn(4.11)) in this limit arises from the behavior of the  $\Gamma_q$  function, which enters both the density of states eq(4.11) and the averaged matrix elements eq(4.14). In the small- $\lambda$  limit (up to non-perturbative corrections), one has [40]

$$\lim_{\lambda \rightarrow 0} \frac{(1-q)^2 (q; q)_\infty^3 q^{\frac{1}{8}}}{|\Gamma_q(\frac{2i\theta}{\lambda})|^2} = 8 \sqrt{\frac{2\pi}{\lambda}} e^{-\frac{2\pi^2}{\lambda} - \frac{2(\frac{\pi}{2} - \theta)^2}{\lambda}} \sin(\theta) \sinh\left(\frac{2\pi\theta}{\lambda}\right) \sinh\left(\frac{2\pi(\pi - \theta)}{\lambda}\right). \quad (\text{C.1})$$

From this, the density of states  $\rho(E) = \frac{\Psi(\theta)}{E_0 \sin \theta}$  (see eq(4.10)) takes a simplified form in two distinct limits<sup>27</sup> given in the main text which we reproduce below,

$$\frac{\Psi(\theta)}{E_0 \sin \theta} = \begin{cases} \frac{2\sqrt{2\pi}}{\lambda} e^{-\frac{\pi^2}{2\lambda}} \theta & \text{for } \theta \ll \lambda \\ \sqrt{\frac{2}{\pi}} e^{-\frac{2}{\lambda}(\frac{\pi}{2} - \theta)^2} & \text{for } \theta \gg \lambda \end{cases}$$

Given the simple expression for density of states, we can now turn to computing physical observables such as partition function and two point function.

**Partition function** The partition function eq(2.3) can be studied in two distinct regimes,  $\beta \ll \lambda^{-3/2}$  and  $\beta \gg \lambda^{-3/2}$ , corresponding to high and low temperatures, respectively. These regimes are characterized by the dominance of different regions of the spectrum. In particular, when  $\beta \gg \lambda^{-3/2}$ , the contribution to the partition function (and hence the two-point function) is dominated by states with  $\theta \ll \lambda$ . This is because,

---

<sup>26</sup>Using the n-orthogonality of  $q$  Hermite polynomials, note the identity,

$$\sum_{k=0}^{\infty} (\pm \tilde{q})^k \frac{H_k^2(1|q)}{(q; q)_k} = \frac{(\tilde{q}^2; q)_\infty}{(\pm \tilde{q}; q)_\infty}.$$

<sup>27</sup>We use  $\lim_{\lambda \rightarrow 0} (q, q)_\infty^3 = \left(\frac{2\pi}{\lambda}\right)^{\frac{3}{2}} e^{-\pi^2/(2\lambda)}$  with  $q = e^{-\lambda}$ . Notably, in the limit  $\lambda \rightarrow 0$ ,  $E - E_0 \sim \lambda^{\frac{3}{2}}$ , the density of states reduces to the well-known sinh form characteristic of the Schwarzian theory.

in this limit, the thermal factor  $e^{-\beta E(\theta)}$  strongly suppresses contributions from higher-energy states, and for small  $\theta$  one has  $E(\theta) \approx -E_0 + \frac{E_0}{2}\theta^2$ , so the weight behaves as  $e^{\beta E_0} e^{-\frac{\beta E_0}{2}\theta^2}$ , effectively cutting off the integral at  $\theta \sim (\beta E_0)^{-1/2} \ll \lambda$ , ensuring that only states with  $\theta \ll \lambda$  contribute significantly. Note that the density of states in this region then matches that of the cold random matrix theory (RMT), implying that the resulting physics in this regime is identical to that of the cold RMT case discussed in Section 3.1.1.

In the remainder of this appendix, we turn our attention to the opposite regime,  $\beta \ll \lambda^{-3/2}$ , where the physics is governed by a different part of the spectrum. To analyze this limit systematically, we consider  $\lambda \rightarrow 0$  while keeping  $\beta\sqrt{\lambda}$  fixed. In this regime, it is self-consistent to assume that the dominant contribution to the partition function arises from the region  $\theta \gg \lambda$ . This allows us to use the simplified form of the density of states given in eq(4.21), leading to the following expression for the partition function:

$$Z(\beta) \approx \sqrt{\frac{2}{\pi\lambda}} \int_0^\pi d\theta \sin \theta e^{\frac{1}{\lambda}(-2(\frac{\pi}{2}-\theta)^2 + \beta E_0 \lambda \cos \theta)} \quad (\text{C.2})$$

Since  $\lambda \rightarrow 0$ , the above integral has a saddle at  $\theta = \theta_0$ , where  $\theta_0$  is given by [39],

$$\frac{\pi}{2} - \theta_0 = \frac{\beta E_0 \lambda}{4} \sin \theta_0 \quad (\text{C.3})$$

It is also convenient to re-express the saddle point equation in terms of another variable  $\phi$ , defined by  $\phi + \theta = \frac{\pi}{2}$  as given in eq(4.22). It is to be noted that  $\theta_0$  only depends on combination  $\beta E_0 \lambda \sim \beta\sqrt{\lambda}$  which is held fixed in the  $\lambda \rightarrow 0$ . To be self consistent with the assumption that the partition function gets contribution only from  $\theta \gg \lambda$  region, we need to ensure  $\theta_0 \gg \lambda$ , i.e.,  $\beta E_0 \lambda \ll \lambda^{-1}$ , i.e.,  $\beta \ll \lambda^{-\frac{3}{2}}$  which is obeyed since  $\beta \sim \frac{1}{\sqrt{\lambda}}$ . Note that for certain limits, the saddle equation can be solved explicitly as below

$$\theta_0 = \begin{cases} \frac{2\pi}{\beta E_0 \lambda} & \beta E_0 \lambda \gg 1 \\ \frac{\pi}{2} - \frac{\beta E_0 \lambda}{4} & \beta E_0 \lambda \ll 1 \end{cases} \quad (\text{C.4})$$

Since  $E_0 \sim \frac{1}{\sqrt{\lambda}}$ , we will refer to the DSSYK regime with  $\frac{1}{\lambda^{\frac{3}{2}}} \gg \beta \gg \frac{1}{\sqrt{\lambda}}$  regime as the low temperature conformal regime and DSSYK regime with  $\beta \ll \frac{1}{\sqrt{\lambda}}$  regime as the high temperature conformal regime. The low temp conformal regime has overlaps with the high temperature Schwarzian theory obtained in the tripled scaling limit mentioned earlier since the region  $\frac{1}{\lambda^{\frac{3}{2}}} \gg \beta \gg \frac{1}{\lambda^{\frac{1}{2}}}$  is accessible from both sides.

**Two point function** Before turning to solving the two point function in this limit we first note the frequency-space two-point function  $\tilde{G}(\omega)$  (using eqn(2.5)), represented as an integral over  $\theta$

$$\tilde{G}(\omega) = \frac{1}{Z(\beta)} \int d\theta \Psi(\theta) e^{\beta E_0 \cos \theta} g(\theta, \theta_\omega) \quad (\text{C.5})$$

where  $\theta_\omega = \arccos\left(\cos \theta - \frac{\omega}{E_0}\right) - \theta$  and the insertion factor  $g(\theta, \theta_\omega)$  is as follows

$$g(\theta, \theta_\omega) \equiv \frac{|(e^{i(2\theta+\theta_\omega)}, q)_m \Gamma_q(\frac{i(2\theta+\theta_\omega)}{\lambda}) \Gamma_q(m + \frac{i\theta_\omega}{\lambda})|^2}{E_0(1-q) \sin \theta \Gamma_q(2m) |\Gamma_q(\frac{2i(\theta+\theta_\omega)}{\lambda})|^2} \quad (\text{C.6})$$

Having established the general form of the frequency-space two-point function  $\tilde{G}(\omega)$  in eq(C.5), we now focus on its behavior in the  $\lambda \rightarrow 0$  limit, which is relevant in the regime  $\beta \ll \lambda^{-3/2}$  discussed earlier. To simplify the analysis, we first consider the case  $\omega = 0$ , which already captures the essential features of the small- $\omega$  physics. For  $\omega = 0$  (i.e.,  $\theta_\omega = 0$ ), since the partition function already has a saddle at  $\theta_0$ <sup>28</sup> given by eq(C.3), the insertion factor  $g$  given in eq(C.6) evaluates to a constant and we have the result<sup>29</sup>

$$\tilde{G}(\omega = 0) = \frac{|(e^{2i\theta_0}, q)_m|^2 \Gamma(m)^2}{E_0 \lambda \sin \theta_0 \Gamma(2m)} = \frac{2(2 \sin \theta_0)^{2m-1} \Gamma(m)^2}{E_0 \lambda \Gamma(2m)} \quad (\text{C.7})$$

where we have used  $|(e^{2i\theta}, q)_m|^2 = (2 \sin \theta)^{2m}$  for  $\theta \gg \lambda$  at small  $\lambda$ . We will now evaluate  $\tilde{G}(\omega)$  for small  $\omega$  with  $\frac{\omega}{E_0 \lambda}$  held fixed (or equivalently  $\omega \beta$  held fixed) as  $\lambda \rightarrow 0$ . In this case, one can solve for  $\theta_\omega = \frac{\omega}{E_0 \sin \theta}$  - note that  $\theta_\omega \sim \mathcal{O}(\lambda)$ . As seen before, the saddle does not shift from  $\theta_0$ . As for the  $\omega = 0$  case, the insertion factor  $g$  given in eq(C.6) evaluates to a constant and we have the result<sup>30</sup>

$$\tilde{G}(\omega) = \frac{2(2 \sin \theta_0)^{2m-1}}{E_0 \lambda \Gamma(2m)} e^{\frac{\beta \omega}{2}} \Gamma(m + \frac{i\omega}{\lambda E_0 \sin \theta_0}) \Gamma(m - \frac{i\omega}{\lambda E_0 \sin \theta_0}) \quad (\text{C.8})$$

---

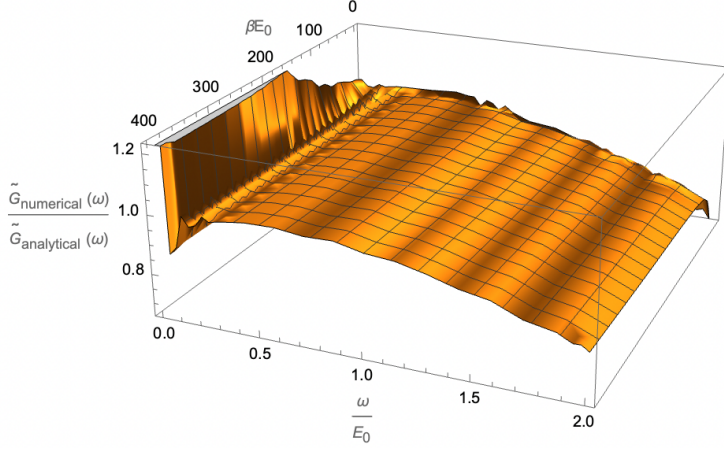
<sup>28</sup>Since there are no exponential in  $\theta$  pieces in the insertion factor  $g$  given in eq(C.6), the saddle for the two point function eq(C.5) does not shift from the saddle of partition function  $\theta_0$  given in eq(C.3). This argument continues to hold in the case of  $\omega \neq 0$ .

<sup>29</sup>Recall that  $\lim_{q \rightarrow 1} \Gamma_q(m) = \Gamma(m)$  for finite  $m$ .

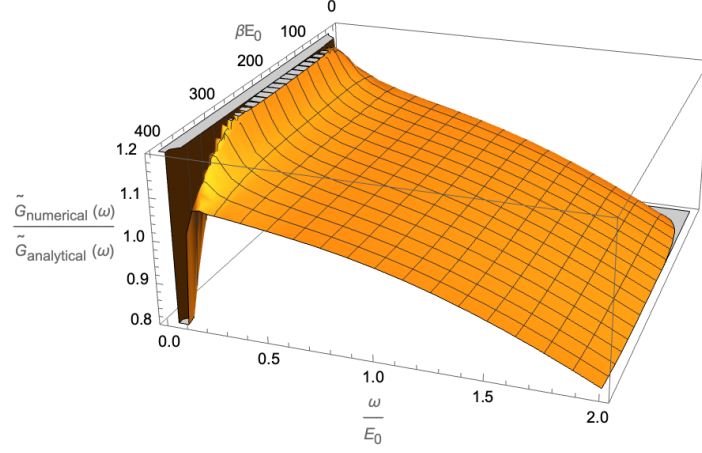
<sup>30</sup>Apart from the explicit factor  $\Gamma(m)^2 \rightarrow |\Gamma(m + \frac{i\theta_\omega}{\lambda})|^2$  the extra factor compared to  $\omega = 0$  case is

$$\frac{|(e^{i(2\theta_0+\theta_\omega)}, q)_m|^2 |\Gamma_q(\frac{i(2\theta_0+\theta_\omega)}{\lambda})|^2}{|(e^{2i\theta_0}, q)_m|^2 |\Gamma_q(\frac{i(2\theta_0+2\theta_\omega)}{\lambda})|^2} \approx \frac{\sin^{2m-1}(\theta_0 + \frac{\theta_\omega}{2}) \sin(\theta_0 + \theta_\omega)}{\sin^{2m}(\theta_0)} e^{\frac{\theta_\omega(\pi-2\theta_0)}{\lambda}} e^{-\frac{3\theta_\omega^2}{2\lambda}}$$

where we have used eq(C.1). The above expression evaluates to  $e^{\frac{\beta \omega}{2}}$  for small  $\theta_\omega \sim \mathcal{O}(\lambda)$  upon using the saddle equation eq(C.3).



(a)  $m = 1$



(b)  $m = 2$

**Figure 25:** Ratio of numerical values of  $\tilde{G}(\omega)$  against analytical result(eq(C.8)) for  $\lambda = 0.05$  and different values of  $m$ .

Note that eq(C.8) is consistent with [58]<sup>31</sup>. In terms of the variable  $\phi$  introduced earlier, the two-point function can be written as shown in eq(4.23). We can confirm that the above analytical result is consistent with numerical results even for slightly large  $\lambda$  and a wide range of  $\beta$  beyond the expected regime  $\beta E_0 \sim \frac{1}{\lambda}$ . In fig(25), we observe that the analytical expression agrees with the numerical data across a broad range of  $\omega$ , with an accuracy of approximately 20%.

<sup>31</sup>With the identification  $v = 1 - \frac{2}{\pi}\theta$ , the Fourier transform of their result for  $G(t)$  exactly matches eq(C.8).

## References

- [1] R. Zwanzig, *Nonequilibrium Statistical Mechanics*. OUP USA, 2001.
- [2] J. I. Kapusta and C. Gale, *Finite-temperature field theory: Principles and applications*. Cambridge Monographs on Mathematical Physics, Cambridge University Press, 2011.
- [3] A. Kamenev, *Field Theory of Non-Equilibrium Systems*. Cambridge University Press, 2011.
- [4] V. Balakrishnan, *Elements of Nonequilibrium Statistical Mechanics*. Springer International Publishing, 2020.
- [5] D. Bernard and B. Doyon, “Energy flow in non-equilibrium conformal field theory,” *J. Phys. A*, vol. 45, p. 362001, 2012.
- [6] A. Almheiri, A. Milekhin, and B. Swingle, “Universal constraints on energy flow and syk thermalization,” *JHEP*, vol. 04, p. 245, 2020.
- [7] D. Bernard and B. Doyon, “Conformal field theory out of equilibrium: a review,” *J. Stat. Mech.*, vol. 1606, no. 6, p. 064005, 2016.
- [8] F. H. L. Essler, G. Mussardo, and M. Panfil, “Generalized Gibbs Ensembles for Quantum Field Theories,” *Phys. Rev. A*, vol. 91, no. 5, p. 051602, 2015.
- [9] A. Dhar, K. Saito, and P. Hänggi, “Nonequilibrium density-matrix description of steady-state quantum transport,” *Phys. Rev. E*, vol. 85, p. 011126, January 2012.
- [10] B. Doyon, “Nonequilibrium density matrix for thermal transport in quantum field theory,” *Communications in Mathematical Physics*, vol. 351, no. 1, pp. 155–200, 2017.
- [11] C. Karrasch, R. Ilan, and J. E. Moore, “Nonequilibrium thermal transport and its relation to linear response,” *Phys. Rev. B*, vol. 88, p. 195129, Nov 2013.
- [12] A. De Luca, J. Viti, L. Mazza, and D. Rossini, “Energy transport in heisenberg chains beyond the luttinger liquid paradigm,” *Phys. Rev. B*, vol. 90, p. 161101, Oct 2014.
- [13] A. Biella, A. De Luca, J. Viti, D. Rossini, L. Mazza, and R. Fazio, “Energy transport between two integrable spin chains,” *Phys. Rev. B*, vol. 93, p. 205121, May 2016.
- [14] A. Biella, M. Collura, D. Rossini, A. De Luca, and L. Mazza, “Ballistic transport and boundary resistances in inhomogeneous quantum spin chains,” *Nature Commun.*, vol. 10, no. 1, p. 4820, 2019.
- [15] B. Bertini, F. Heidrich-Meisner, C. Karrasch, T. Prosen, R. Steinigeweg, and M. Žnidarič, “Finite-temperature transport in one-dimensional quantum lattice models,” *Rev. Mod. Phys.*, vol. 93, p. 025003, May 2021.
- [16] S. A. Hartnoll, A. Lucas, and S. Sachdev, *Holographic quantum matter*. MIT press, 2018.

- [17] A. Kitaev, “A simple model of quantum holography.”  
<http://online.kitp.ucsb.edu/online/entangled15/kitaev/>, 2015.
- [18] S. Sachdev and J. Ye, “Gapless spin-fluid ground state in a random quantum heisenberg magnet,” *Phys. Rev. Lett.*, vol. 70, pp. 3339–3342, May 1993.
- [19] J. Maldacena and D. Stanford, “Remarks on the sachdev-ye-kitaev model,” *Phys. Rev. D*, vol. 94, p. 106002, Nov 2016.
- [20] J. Polchinski and V. Rosenhaus, “The spectrum in the sachdev-ye-kitaev model,” *Journal of High Energy Physics*, vol. 2016, pp. 1–25, 2016.
- [21] S. Sachdev, “Strange metals and the AdS/CFT correspondence,” *J. Stat. Mech.*, vol. 1011, p. P11022, 2010.
- [22] J. Maldacena, S. H. Shenker, and D. Stanford, “A bound on chaos,” *JHEP*, vol. 08, p. 106, 2016.
- [23] J. Maldacena, D. Stanford, and Z. Yang, “Conformal symmetry and its breaking in two dimensional Nearly Anti-de-Sitter space,” *PTEP*, vol. 2016, no. 12, p. 12C104, 2016.
- [24] J. Engelsöy, T. G. Mertens, and H. Verlinde, “An investigation of AdS<sub>2</sub> backreaction and holography,” *JHEP*, vol. 07, p. 139, 2016.
- [25] S. Sachdev, “Bekenstein-hawking entropy and strange metals,” *Phys. Rev. X*, vol. 5, p. 041025, Nov 2015.
- [26] D. J. Gross and V. Rosenhaus, “A Generalization of Sachdev-Ye-Kitaev,” *JHEP*, vol. 02, p. 093, 2017.
- [27] J. Yoon, “SYK Models and SYK-like Tensor Models with Global Symmetry,” *JHEP*, vol. 10, p. 183, 2017.
- [28] P. Narayan and J. Yoon, “Supersymmetric syk model with global symmetry,” *Journal of High Energy Physics*, vol. 2018, pp. 1–60, 2018.
- [29] Y. Gu, A. Y. Kitaev, S. Sachdev, and G. M. Tarnopolsky, “Notes on the complex sachdev-ye-kitaev model,” *Journal of High Energy Physics*, vol. 2020, pp. 1–74, 2020.
- [30] R. Bhattacharya, S. Chakrabarti, D. P. Jatkar, and A. Kundu, “Syk model, chaos and conserved charge,” *Journal of High Energy Physics*, vol. 2017, pp. 1–16, 2017.
- [31] J. Liu and Y. Zhou, “Note on global symmetry and SYK model,” *JHEP*, vol. 05, p. 099, 2019.
- [32] W. Fu, D. Gaiotto, J. Maldacena, and S. Sachdev, “Supersymmetric sachdev-ye-kitaev models,” *Phys. Rev. D*, vol. 95, p. 026009, Jan 2017.
- [33] J. Yoon, “Supersymmetric syk model: bi-local collective superfield/supermatrix formulation,” *Journal of High Energy Physics*, vol. 2017, pp. 1–48, 2017.

- [34] C. Peng, M. Spradlin, and A. Volovich, “Correlators in the  $\mathcal{N} = 2$  Supersymmetric SYK Model,” *JHEP*, vol. 10, p. 202, 2017.
- [35] A. Larzul and M. Schirò, “Energy transport across two interacting quantum baths without quasiparticles,” *Phys. Rev. B*, vol. 108, p. 115120, Sep 2023.
- [36] A. Larzul, S. J. Thomson, and M. Schirò, “Are fast scramblers good thermal baths?,” Apr. 2022.
- [37] L. Erdős and D. Schröder, “Phase transition in the density of states of quantum spin glasses,” *Mathematical Physics, Analysis and Geometry*, vol. 17, pp. 441–464, 2014.
- [38] J. S. Cotler, G. Gur-Ari, M. Hanada, J. Polchinski, P. Saad, S. H. Shenker, D. Stanford, A. Streicher, and M. Tezuka, “Black Holes and Random Matrices,” *JHEP*, vol. 05, p. 118, 2017. [Erratum: *JHEP* 09, 002 (2018)].
- [39] M. Berkooz, P. Narayan, and J. Simón, “Chord diagrams, exact correlators in spin glasses and black hole bulk reconstruction,” *Journal of High Energy Physics*, vol. 2018, p. 192, Aug. 2018.
- [40] M. Berkooz, M. Isachenkov, V. Narovlansky, and G. Torrents, “Towards a full solution of the large  $N$  double-scaled SYK model,” *JHEP*, vol. 03, p. 079, 2019.
- [41] M. Berkooz, N. Brukner, V. Narovlansky, and A. Raz, “Multi-trace correlators in the SYK model and non-geometric wormholes,” *JHEP*, vol. 21, p. 196, 2020.
- [42] H. W. Lin, “The bulk Hilbert space of double scaled SYK,” *JHEP*, vol. 11, p. 060, 2022.
- [43] M. Berkooz, M. Isachenkov, M. Isachenkov, P. Narayan, and V. Narovlansky, “Quantum groups, non-commutative  $\text{AdS}_2$ , and chords in the double-scaled SYK model,” *JHEP*, vol. 08, p. 076, 2023.
- [44] T. G. Mertens and G. J. Turiaci, “Solvable models of quantum black holes: a review on Jackiw–Teitelboim gravity,” *Living Rev. Rel.*, vol. 26, no. 1, p. 4, 2023.
- [45] L. Susskind, “Entanglement and Chaos in De Sitter Space Holography: An SYK Example,” *JHAP*, vol. 1, no. 1, pp. 1–22, 2021.
- [46] L. Susskind, “De sitter space, double-scaled syk, and the separation of scales in the semiclassical limit,” *Journal of Holography Applications in Physics*, vol. 5, no. 1, pp. 1–30, 2025.
- [47] L. Susskind, “Scrambling in double-scaled syk and de sitter space,” May 2022.
- [48] A. Blommaert, T. G. Mertens, and J. Papalini, “The dilaton gravity hologram of double-scaled SYK,” *JHEP*, vol. 06, p. 050, 2025.
- [49] P. Narayan and S. T. S, “SYK Model with global symmetries in the double scaling limit,” *JHEP*, vol. 05, p. 083, 2023.

- [50] M. Berkooz, V. Narovlansky, and H. Raj, “Complex sachdev-ye-kitaev model in the double scaling limit,” *arXiv: High Energy Physics - Theory*, 2020.
- [51] M. Berkooz, N. Brukner, V. Narovlansky, and A. Raz, “The double scaled limit of Super-Symmetric SYK models,” *JHEP*, vol. 12, p. 110, 2020.
- [52] J. Maldacena and D. Stanford, “Remarks on the Sachdev-Ye-Kitaev model,” *Phys. Rev. D*, vol. 94, no. 10, p. 106002, 2016.
- [53] D. Chakrabarti and G. K. Srinivasan, “On a remarkable formula of ramanujan,” *Archiv der Mathematik*, vol. 99, pp. 125–135, Aug. 2012.
- [54] M. Dodelson, “Ringdown in the syk model,” Aug. 2024. CERN-TH-2024-135.
- [55] M. Berkooz and O. Mamroud, “A cordial introduction to double scaled syk,” *arXiv.org*, July 2024.
- [56] Wikipedia, “Continuous q-Hermite polynomials — Wikipedia, the free encyclopedia.” <http://en.wikipedia.org/w/index.php?title=Continuous%20q-Hermite%20polynomials&oldid=1121109966>.
- [57] R. Koekoek, T. Koornwinder, P. Lesky, and R. Swarttouw, *Hypergeometric Orthogonal Polynomials and Their q-Analogues*. Springer Monographs in Mathematics, Springer Berlin Heidelberg, 2010.
- [58] B. Mukhametzhanov, “Large p SYK from chord diagrams,” *JHEP*, vol. 09, p. 154, 2023.
- [59] A. Goel, V. Narovlansky, and H. Verlinde, “Semiclassical geometry in double-scaled SYK,” *JHEP*, vol. 11, p. 093, 2023.
- [60] Y. Gu, X.-L. Qi, and D. Stanford, “Local criticality, diffusion and chaos in generalized sachdev-ye-kitaev models,” *Journal of High Energy Physics*, vol. 2017, May 2017.
- [61] M. Bucca and M. Mezei, “Nonlinear soft mode action for the large- $p$  syk model,” 2024.
- [62] I. S. Gradshteyn and I. M. Ryzhik, *Table of integrals, series, and products*. Elsevier/Academic Press, Amsterdam, seventh ed., 2007.